promotes cardiogenesis by maintaining the proliferation and/or survival of embryonic cardiomyocytes.

It has been shown that canonical Wnt signals inhibit cardiogenesis in chick and frog embryos, and that Wnt antagonists such as Dkk1 and Crescent secreted from the anterior endoderm or the organizer region counteract the Wnt-mediated inhibitory signals and induce cardiogenesis in the anterior lateral mesoderm[4]. However, IGFBP-4-mediated Wnt inhibition is required at later stages of development, when the heart is already formed at the ventral portion and starts to grow and remodel to maintain embryonic circulation. It has been shown that Wnt/β-catenin signalling has time-dependent effects on cardiogenesis in ES cells: canonical Wnt signalling in the early phase of ES-cell differentiation promotes cardiomyogenesis, whereas it inhibits cardiomyocyte differentiation in the late phase[10–12]. In agreement with this notion, IGFBP-4 promoted cardiomyocyte differentiation of ES cells only when IGFBP-4 was applied in the late phase after embryoid body formation (Supplementary Fig. 3a–c). Similar time-dependent effects of Wnt/β-catenin signalling on cardiogenesis has been shown in zebrafish embryos[11]. Moreover, several recent reports suggest that Wnt/β-catenin signalling is a positive regulator of cardiac progenitor-cell proliferation in the secondary heart field[13]. It therefore seems that canonical Wnt signalling has divergent effects on cardiogenesis at multiple stages of development: first, canonical Wnt signalling promotes cardiogenesis at the time of gastrulation or mesoderm specification; second, it inhibits cardiogenesis at the time when cardiac mesoderm is specified in the anterior lateral mesoderm; third, it promotes the expansion of cardiac progenitors in the secondary heart field; and fourth, it inhibits cardiogenesis at later stages when the embryonic heart is growing. It is interesting to note that IGFBP-4 is expressed predominantly in the liver. Mouse IGFBP-4 is

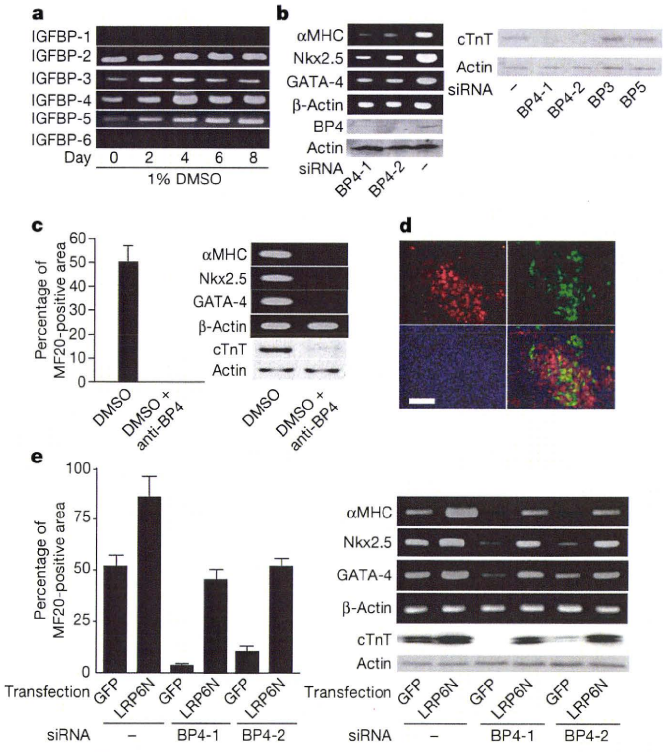

Figure 3 | IGFBP-4 is required for the differentiation of P19CL6 cells into cardiomyocytes. a, Expression analysis of IGFBP family members by RT–PCR during DMSO-induced cardiomyocyte differentiation of P19CL6 cells (from day 0 to day 8). **b**, Left: knockdown of *Igfbp4* in P19CL6 cells attenuated cardiac marker expression in response to treatment with DMSO. BP4-1 and BP4-2 represent two different siRNAs for IGFBP-4. Right: knockdown of *Igfbp3* or *Igfbp5* had no effect on cTnT expression in response to DMSO treatment. **c**, Treatment with a neutralizing antibody against IGFBP-4 (anti-BP4; 40 μg ml^{-1}) attenuated DMSO-induced cardiomyocyte differentiation of P19CL6 cells. Error bars show s.d. **d**, IGFBP-4 immunostaining during DMSO-induced differentiation of P19CL6 cells stably transfected with αMHC–green fluorescent protein (GFP) reporter gene. Top left, IGFBP-4 staining (red); top right, GFP expression representing differentiated cardiomyocytes; bottom left, nuclear staining with DAPI (4′,6-diamidino-2-phenylindole); bottom right, a merged picture. Scale bar, 100 μm. **e**, Attenuated cardiomyocyte differentiation of P19CL6 cells by *Igfbp4* knockdown was rescued by inhibiting Wnt/β-catenin signalling. Control and *Igfbp4*-knocked-down P19CL6 cells were transfected with an expression vector for GFP or LRP6N (a dominant-negative form of LRP6) and induced to differentiate into cardiomyocytes by treatment with DMSO. LRP6N overexpression rescued the attenuated cardiomyocyte differentiation induced by *Igfbp4* knockdown as assessed by MF20-positive area (left panel), cardiac marker-gene expression and cTnT protein expression (right panel). Error bars show s.d.

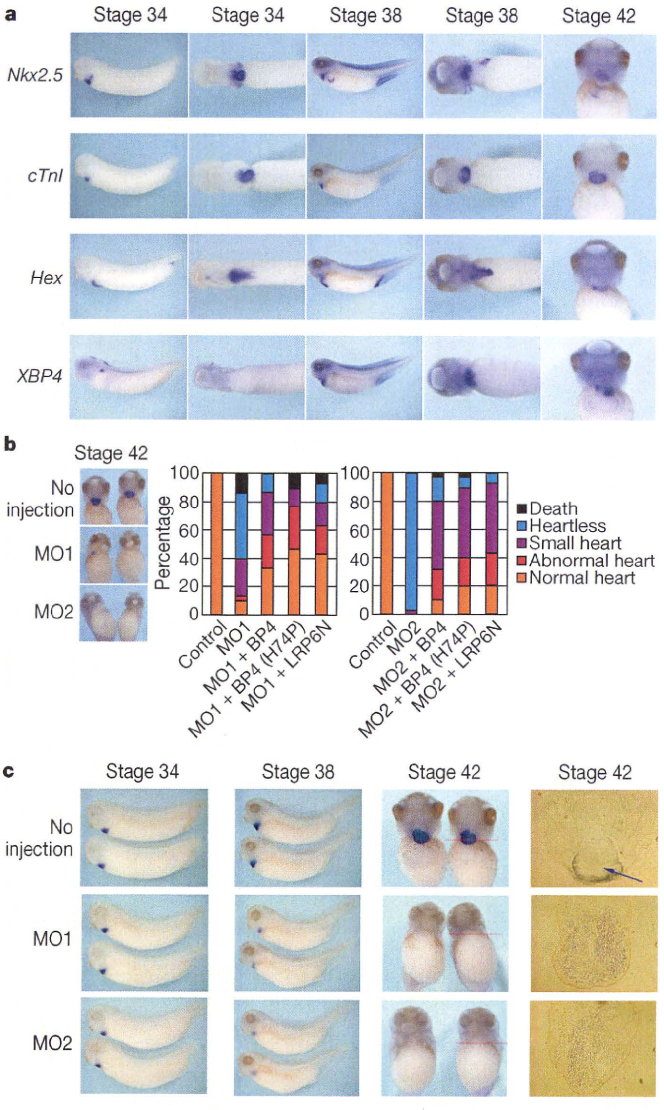

Figure 4 | IGFBP-4 is required for the maturation of the heart in *Xenopus* embryos. a, *In situ* hybridization analysis of *Nkx2.5* (an early cardiac marker), *cTnI* (a mature cardiac marker), *Hex* (a liver marker), and *XIGFBP-4* (*XBP4*) mRNA expression at stages 34, 38 and 42. **b**, Knockdown of *XIGFBP-4* by two different morpholinos (MO1 and MO2) resulted in severe cardiac defects as assessed by *cTnI in situ* hybridization at stage 42 (left). These cardiac defects were rescued by simultaneous injection of MO-resistant wild-type XIGFBP-4, mutant XIGFBP-4-H74P (BP4(H74P) and LRP6N ($n = 30$ for each group). **c**, Temporal profile of cardiac defects induced by *XIGFBP-4* knockdown. Morphology of the heart as assessed by cTnI *in situ* hybridization was almost normal at stage 34 but was severely perturbed at stages 38 and 42. The right column shows sections of control and MO-injected embryos. The arrow indicates the heart in control embryos. No heart-like structure was observed in MO-injected embryos.

©2008 Macmillan Publishers Limited. All rights reserved

also strongly expressed in the tissues adjacent to the heart such as pharyngeal arches and liver bud at embryonic day (E)9.5 (Supplementary Fig. 3h). These observations and the results of IGFBP-4 immunostaining in P19CL6 cells and ES cells suggest that IGFBP-4 promotes cardiogenesis in a paracrine fashion. Together with a previous report showing that cardiac mesoderm secretes FGFs and induces liver progenitors in the ventral endoderm[14], these observations suggest that there exist reciprocal paracrine signals between the heart and the liver that coordinately promote the development of each other.

IGFBPs are composed of six members, IGFBP-1 to IGFBP-6. Reporter gene assays and β-catenin stabilization assays revealed that IGFBP-4 was the most potent canonical Wnt inhibitor and that IGFBP-1, IGFBP-2 and IGFBP-6 also showed modest activity in Wnt inhibition, whereas IGFBP-3 and IGFBP-5 had no such activity (Supplementary Fig. 5a–c). In agreement with this, IP/western blot analyses demonstrated that IGFBP-1, IGFBP-2, IGFBP-4 and IGFBP-6 but not IGFBP-3 or IGFBP-5 interacted with LRP6 or Frz8CRD (Supplementary Fig. 5d, e). Thus, the lack of cardiac phenotypes in IGFBP-4-null mice or IGFBP-3/IGFBP-4/IGFBP-5 triple knockout mice[15] may be due to genetic redundancies between IGFBP-4 and other IGFBPs such as IGFBP-1, IGFBP-2 and/or IGFBP-6.

The identification of IGFBP-4 as an inhibitor of Wnt/β-catenin signalling may also have some implications for cancer biology[16]. It was shown that treatment with IGFBP-4 reduces cell proliferation in some cancer cell lines *in vitro*, and that overexpression of IGFBP-4 attenuates the growth of prostate cancer *in vivo*. Decreased serum levels of IGFBP-4 are associated with the risk of breast cancer. Because the activation of Wnt signalling is implicated in several forms of malignant tumours[17,18], it is possible that the inhibitory effect of IGFBP-4 on cell proliferation is mediated in part by the inhibition of canonical Wnt signalling.

METHODS SUMMARY

Cell culture. P19CL6 cells and ES cells were cultured and induced to differentiate into cardiomyocytes essentially as described[6,10]. P19CL6 cells (2,000 cells per 35-mm dish) were treated with various conditioned media for screening of their cardiogenic activities. For siRNA-mediated knockdown, pSIREN-RetroQ vectors (Clontech) ligated with double-stranded oligonucleotides were transfected into P19CL6 cells or ES cells, and puromycin-resistant clones were selected.

IP/western blot analyses and binding assays. Conditioned media for IP/western blot analyses were produced by using 293 cells. Binding reactions were performed overnight at 4 °C. ^{125}I-labelling of IGFBP-4 and Wnt3A was performed with IODO-BEADS Iodination Reagent (Pierce). A liquid-phase binding assay was performed essentially as described[19].

***Xenopus* experiments.** Axis duplication assays, animal cap assays, and *in situ* hybridization analyses in *Xenopus* were performed essentially as described[20]. Electroporation of mRNA was performed at stage 28 essentially as described[21].

Full Methods and any associated references are available in the online version of the paper at www.nature.com/nature.

Received 22 August 2007; accepted 24 April 2008.
Published online 4 June 2008.

1. Firth, S. M. & Baxter, R. C. Cellular actions of the insulin-like growth factor binding proteins. *Endocr. Rev.* **23**, 824–854 (2002).
2. Mohan, S. & Baylink, D. J. IGF-binding proteins are multifunctional and act via IGF-dependent and -independent mechanisms. *J. Endocrinol.* **175**, 19–31 (2002).
3. Olson, E. N. & Schneider, M. D. Sizing up the heart: development redux in disease. *Genes Dev.* **17**, 1937–1956 (2003).
4. Foley, A. & Mercola, M. Heart induction: embryology to cardiomyocyte regeneration. *Trends Cardiovasc. Med.* **14**, 121–125 (2004).
5. Leri, A., Kajstura, J. & Anversa, P. Cardiac stem cells and mechanisms of myocardial regeneration. *Physiol. Rev.* **85**, 1373–1416 (2005).
6. Monzen, K. *et al.* Bone morphogenetic proteins induce cardiomyocyte differentiation through the mitogen-activated protein kinase kinase kinase TAK1 and cardiac transcription factors Csx/Nkx-2.5 and GATA-4. *Mol. Cell. Biol.* **19**, 7096–7105 (1999).
7. Ueno, H. *et al.* A stromal cell-derived membrane protein that supports hematopoietic stem cells. *Nature Immunol.* **4**, 457–463 (2003).
8. Qin, X., Strong, D. D., Baylink, D. J. & Mohan, S. Structure–function analysis of the human insulin-like growth factor binding protein-4. *J. Biol. Chem.* **273**, 23509–23516 (1998).
9. Moon, R. T., Kohn, A. D., De Ferrari, G. V. & Kaykas, A. WNT and β-catenin signalling: diseases and therapies. *Nature Rev. Genet.* **5**, 691–701 (2004).
10. Naito, A. T. *et al.* Developmental stage-specific biphasic roles of Wnt/β-catenin signaling in cardiomyogenesis and hematopoiesis. *Proc. Natl Acad. Sci. USA* **103**, 19812–19817 (2006).
11. Ueno, S. *et al.* Biphasic role for Wnt/β-catenin signaling in cardiac specification in zebrafish and embryonic stem cells. *Proc. Natl Acad. Sci. USA* **104**, 9685–9690 (2007).
12. Liu, Y. *et al.* Sox17 is essential for the specification of cardiac mesoderm in embryonic stem cells. *Proc. Natl Acad. Sci. USA* **104**, 3859–3864 (2007).
13. Cohen, E. D., Tian, Y. & Morrisey, E. E. Wnt signaling: an essential regulator of cardiovascular differentiation, morphogenesis and progenitor self-renewal. *Development* **135**, 789–798 (2008).
14. Jung, J., Zheng, M., Goldfarb, M. & Zaret, K. S. Initiation of mammalian liver development from endoderm by fibroblast growth factors. *Science* **284**, 1998–2003 (1999).
15. Ning, Y. *et al.* Diminished growth and enhanced glucose metabolism in triple knockout mice containing mutations of insulin-like growth factor binding protein-3, -4, and -5. *Mol. Endocrinol.* **20**, 2173–2186 (2006).
16. Durai, R. *et al.* Biology of insulin-like growth factor binding protein-4 and its role in cancer. *Int. J. Oncol.* **28**, 1317–1325 (2006).
17. Logan, C. Y. & Nusse, R. The Wnt signaling pathway in development and disease. *Annu. Rev. Cell Dev. Biol.* **20**, 781–810 (2004).
18. Clevers, H. Wnt/β-catenin signaling in development and disease. *Cell* **127**, 469–480 (2006).
19. Semenov, M. V. *et al.* Head inducer Dickkopf-1 is a ligand for Wnt coreceptor LRP6. *Curr. Biol.* **11**, 951–961 (2001).
20. Kobayashi, H. *et al.* Novel Daple-like protein positively regulates both the Wnt/β-catenin pathway and the Wnt/JNK pathway in *Xenopus*. *Mech. Dev.* **122**, 1138–1153 (2005).
21. Sasagawa, S., Takabatake, T., Takabatake, Y., Muramatsu, T. & Takeshima, K. Improved mRNA electroporation method for *Xenopus* neurula embryos. *Genesis* **33**, 81–85 (2002).

Supplementary Information is linked to the online version of the paper at www.nature.com/nature.

Acknowledgements We thank E. Fujita, R. Kobayashi and Y. Ishiyama for technical support; T. Yamauchi and K. Ueki for advice on binding assays; and Y. Onuma and S. Takahashi for advice on *Xenopus* electroporation. This work was supported by grants from the Ministry of Education, Culture, Sports, Science and Technology (MEXT), the Ministry of Health, Labour, and Welfare, and the New Energy and Industrial Technology Development Organization (NEDO).

Author Contributions W.Z., I.S. and Y.I. contributed equally to this work. I.K. designed and supervised the research. W.Z., I.S., Y.I., Z.L., H.I., M.Y. and A.T.N. performed experiments, J.N., H.U., A.U., T.M., T.N., A.K. and M.A. contributed new reagents and/or analytical tools. W.Z., I.S., Y.I., A.K. and I.K. analysed data. W.Z., I.S., Y.I. and I.K. prepared the manuscript.

Author Information Reprints and permissions information is available at www.nature.com/reprints. Correspondence and requests for materials should be addressed to I.K. (komuro-tky@umin.ac.jp).

©2008 Macmillan Publishers Limited. All rights reserved

METHODS

Plasmids and reagents. cDNA clones encoding mouse IGFBPs and *Xenopus* IGFBP-4 were purchased from Open Biosystems. XIGFBP-4-H74P mutant was generated with a QuickChange Site-Directed Mutagenesis kit (Stratagene). His-tagged human wild-type IGFBP-4 and mutant IGFBP-4-H74P (vectors provided by X. Qin)[8] were produced and purified with HisTrap HP Kit (Amersham). Full-length Frz8, Frz8CRD and LRP6N were provided by X. He[22,23]. Full-length LRP6, membrane-bound forms of LRP6 deletion mutants, and Dkk1 were from C. Niehrs[24]. pXwnt8 and pCSKA-Xwnt8 were from J. Christian[25]. pCS2–β-catenin was from D. Kimelman[26]. αMHC–GFP was from B. Fleischmann[27]. BRE–luc was from P. ten Dijke[28]. pCGN-Dvl-1 was described previously[29]. Soluble forms of LRP6 deletion mutants and probes for *in situ* hybridization analysis (Nkx2.5, cTnI and Hex) were generated by PCR. IGFBP-4, Wnt3A, IGF-I, IGF-II and BMP2 were from R&D. Neutralizing antibodies were from R&D (anti-IGFBP-4), Sigma (anti-IGF-I and anti-IGF-II), and Oncogene (anti-type-I IGF receptor). The antibodies used for immunoprecipitation, western blotting and immunostaining were from Invitrogen (anti-Myc, anti-V5), Santa Cruz (anti-cTnT, anti-IGFBP-4, anti-topoisomerase I (TOPO-I)), Sigma (anti-β-actin, anti-β-catenin, anti-FLAG (M2)) and Developmental Studies Hybridoma Bank (anti-sarcomeric myosin heavy chain (MF20)).

Cell culture experiments. P19CL6 cells and ES cells were cultured and induced to differentiate into cardiomyocytes essentially as described[6,10]. P19CL6 cells (2,000 cells per 35-mm dish) were treated with various conditioned media for screening of their cardiogenic activities. P19CL6 cells or ES cells stably transfected with αMHC promoter driven–GFP were generated by transfection of αMHC–GFP plasmid into P19CL6 cells or ht7 ES cells followed by G418 selection. Luciferase reporter gene assays, western blot analyses, immunostaining and RT–PCR were performed as described[10]. Reporter gene assays were repeated at least three times. PCR primers and PCR conditions are listed in Supplementary Table 1. For siRNA-mediated knockdown, siRNAs were expressed with pSIREN-RetroQ vector (Clontech). Oligonucleotide sequences used are listed in Supplementary Table 2. pSIREN-RetroQ vectors ligated with double-stranded oligonucleotides were transfected into P19CL6 cells or ES cells, and puromycin-resistant clones were isolated and expanded. For β-catenin stabilization assays, nuclear extracts of L cells were prepared with NE-PER Nuclear and Cytoplasmic Extraction Reagents (Pierce). Data are shown as means and s.d.

IP/western blot analyses and binding assays. Conditioned media for IP/western blot analyses containing full-length or various deletion mutants of IGFBPs, LRP6, Frz8CRD and Dkk1 were produced with 293 cells. Binding reactions were performed overnight at 4 °C. Immunoprecipitation was performed with Protein G–Sepharose 4 Fast Flow (Amersham). ^{125}I-labelling of IGFBP-4 and Wnt3A was performed with IODO-BEADS Iodination Reagent (Pierce). A liquid-phase binding assay was performed essentially as described[19]. In brief, conditioned media containing LRP6N–Myc or Frz8CRD–Myc were mixed with various concentrations of ^{125}I-labelled IGFBP-4 and incubated overnight at 4 °C. LRP6N–Myc or Frz8CRD–Myc was immunoprecipitated and the radioactivity of bound IGFBP-4 was measured after extensive washing of the Protein G–Sepharose beads. For a competitive binding assay, conditioned media containing LRP6N–Myc or Frz8CRD–Myc were mixed with ^{125}I-labelled Wnt3A and unlabelled IGFBP-4, and incubated overnight at 4 °C. LRP6N–Myc or Frz8CRD–Myc was then immunoprecipitated and the radioactivity of bound Wnt3A was measured.

***Xenopus* experiments and mouse *in situ* hybridization analysis.** Axis duplication assays, animal cap assays and *in situ* hybridization analyses in *Xenopus* were performed essentially as described[20]. Two independent cDNAs for *XIGFBP-4*, presumably resulting from pseudotetraploid genomes, were identified by 5′ rapid amplification of cDNA ends (Supplementary Fig. 4a). Two different MOs targeting both of these two IGFBP-4 transcripts were designed (Gene Tools) (Supplementary Fig. 4a and Supplementary Table 2). MO-sensitive *XIGFBP-4* cDNA including a 41-base-pair 5′-untranslated region (UTR) was generated by PCR. MO-resistant *XIGFBP-4* cDNA (wild-type and H74P mutant) was generated by introducing five silent mutations in the MO1 target sequence and excluding the 5′-UTR (Supplementary Fig. 4a). To determine the specificity of MOs, MO-sensitive or MO-resistant *XIGFBP-4–myc* mRNA was injected into *Xenopus* embryos with or without MOs, and protein/mRNA expression was analysed. PCR primers and PCR conditions are listed in Supplementary Table 1. MOs and plasmid DNAs were injected at the eight-cell stage into the dorsal region of two dorsal–vegetal blastomeres fated to be heart and liver anlage. Electroporation of mRNA was performed essentially as described[21]. Injection of mRNA (5 ng in 5 nl of solution) into the vicinity of heart anlage and application of electric pulses were performed at stage 28. Whole-mount *in situ* hybridization analysis of murine IGFBP-4 was performed as described[30].

22. He, X. *et al.* A member of the Frizzled protein family mediating axis induction by Wnt-5A. *Science* **275**, 1652–1654 (1997).
23. Tamai, K. *et al.* LDL-receptor-related proteins in Wnt signal transduction. *Nature* **407**, 530–535 (2000).
24. Mao, B. *et al.* LDL-receptor-related protein 6 is a receptor for Dickkopf proteins. *Nature* **411**, 321–325 (2001).
25. Christian, J. L. & Moon, R. T. Interactions between Xwnt-8 and Spemann organizer signaling pathways generate dorsoventral pattern in the embryonic mesoderm of *Xenopus*. *Genes Dev.* **7**, 13–28 (1993).
26. Yost, C. *et al.* The axis-inducing activity, stability, and subcellular distribution of β-catenin is regulated in *Xenopus* embryos by glycogen synthase kinase 3. *Genes Dev.* **10**, 1443–1454 (1996).
27. Kolossov, E. *et al.* Identification and characterization of embryonic stem cell-derived pacemaker and atrial cardiomyocytes. *FASEB J.* **19**, 577–579 (2005).
28. Korchynskyi, O. & ten Dijke, P. Identification and functional characterization of distinct critically important bone morphogenetic protein-specific response elements in the Id1 promoter. *J. Biol. Chem.* **277**, 4883–4891 (2002).
29. Kishida, M. *et al.* Synergistic activation of the Wnt signaling pathway by Dvl and casein kinase Iε. *J. Biol. Chem.* **276**, 33147–33155 (2001).
30. Hosoda, T. *et al.* A novel myocyte-specific gene Midori promotes the differentiation of P19CL6 cells into cardiomyocytes. *J. Biol. Chem.* **276**, 35978–35989 (2001).

©2008 Macmillan Publishers Limited. All rights reserved

Differentiation 77 (2009) 317–323

Contents lists available at ScienceDirect

Differentiation

journal homepage: www.elsevier.com/locate/diff

The multipotency of adult vibrissa follicle stem cells

Alessandro Wataru Amici [a,1], Masayuki Yamato [b], Teruo Okano [b], Koji Kobayashi [c,*]

[a] Graduate School of Science and Technology, Chiba University, Chiba, Japan
[b] Institute of Advanced Biomedical Engineering and Science, Tokyo Women's Medical University, Tokyo, Japan
[c] Department of Biology, Faculty of Science, Chiba University, Chiba, Japan

ARTICLE INFO

Article history:
Received 22 July 2008
Received in revised form
9 September 2008
Accepted 2 October 2008

Keywords:
Hair follicle stem cells
Bulge keratinocyte sheet
Transplantation
Hair follicle induction

ABSTRACT

Several studies focused on the characterization of bulge keratinocytes have proved that they are multipotent stem cells, being recruited not only to regenerate the hair follicle itself, but also the sebaceous gland and the epidermis. However, due to the difficulty in preparing transplantable cell sheets harvested with conventional enzymatic digestion, there is still no direct evidence of the bulge stem cells' multipotency. Whether they can respond to adult dermal papilla (DP) signals in recombination experiments also remains unclear. In this study, we addressed this problem by culturing and detaching intact bulge keratinocyte sheets from thermo-responsive culture dishes, only by reducing its temperature. When sheets of mass cultured bulge keratinocytes isolated from rat vibrissa follicles were recombined with fresh adult DPs and sole skin dermis *in vivo*, regeneration of epidermis and sebaceous gland-like structures, and formation of hair bulb with differentiating inner root sheath and hair cuticle were observed within 3 weeks. However, regardless the expression of stem cells markers like CD34, SA1004 and SA1006, no structures were observed when cloned bulge keratinocytes were used to prepare cell sheets and recombinants, revealing the possible existence of monoclonal stem cells within the bulge region. This report is the first to succeed in harvesting adult bulge keratinocyte sheets. Using these sheets it is demonstrated that bulge stem cells directly respond to adult DP signals to induce hair bulb formation *in vivo*.

© 2008 International Society of Differentiation. Published by Elsevier Ltd. All rights reserved.

1. Introduction

Hair follicles are specialized mammalian skin appendages responsible for hair fiber production. Thanks to their accessibility, many studies have focused and eventually succeeded in the localization, isolation and characterization of hair follicle stem cells. Like other adult stem cells, hair follicle stem cells are assumed to be slow cycling and have superior self-renewal and multipotency abilities (Cotsarelis, 2006). Being able to be detected as label-retaining cells (LRC) (Cotsarelis et al., 1990; Taylor et al., 2000), many studies have demonstrated that in rodent hair follicles, most stem cells are located in the bulge, a swelling in the upper part of the outer root sheath (ORS), with very few in the hair bulb (Kobayashi et al., 1993; Taylor et al., 2000; Oshima et al., 2001; Claudinot et al., 2005). Bulge keratinocytes isolated from vibrissa follicles show high clonogenecity and proliferative capacity *in vitro* (Kobayashi et al., 1993; Oshima et al., 2001; Claudinot et al., 2005) and their multipotency have been demonstrated by studies that followed the fate of LRCs during hair morphogenesis and through the hair growth cycle (Cotsarelis et al., 1990), as well as during skin wound-healing processes (Taylor et al., 2000).

Different tissue recombination and transplantation models using adult bulge keratinocytes have also shown the hair follicle stem cells' multipotency, proving that they are involved in the epidermis and sebaceous gland formation (Oshima et al., 2001; Morris et al., 2004; Blanpain et al., 2004; Claudinot et al., 2005). All these works, however, have utilized embryonic or neonatal cells or tissues in their models, demonstrating only that hair follicle stem cells can be recruited by an environment that is able to develop skin appendages, but showing no direct proof of their ability to reconstruct skin and form its appendages *de novo*.

One of the reasons for this lack of direct evidence is the difficulty in preparing transplantable bulge keratinocyte sheets harvested with conventional enzymatic digestion. In the present study, this problem was addressed by culturing and detaching bulge keratinocyte sheets using a technology that does not require the use of proteolytic enzymes (Yamato et al., 2001). Keratinocytes are plated in culture dishes coated with poly (*N*-isopropylacrylamide), a thermo-responsive polymer that becomes hydrophobic above 32 °C and can reversibly change to hydrophilic below this temperature. Using this technology, multilayered keratinocyte

* Corresponding author. Fax: +81 43 432 5535.
E-mail address: kkoba@air.linkclub.or.jp (K. Kobayashi).
[1] Present address: Laboratory of Stem Cell Dynamics, Ecole Polytechnique Fédérale de Lausanne, Lausanne, Switzerland.

0301-4681/$ - see front matter © 2008 International Society of Differentiation. Published by Elsevier Ltd. All rights reserved.
doi:10.1016/j.diff.2008.10.010

sheets can be detached intact, simply by reducing the dishes temperature to 20 °C. Using this method, we succeeded in demonstrating that cultured adult bulge keratinocytes can construct the epidermis and interact with adult dermal papilla (DPs), forming sebaceous glands and the hair follicle itself *in vivo*. These data indicated that the use of cultured bulge keratinocyte sheets is effective in hair follicle induction experiments and also strongly support the concept that hair follicle stem cells are multipotent, providing direct evidence of this feature.

2. Material and methods

2.1. Animals

Fisher F344/Jcl rats were obtained from Nihon SLC Co. Ltd. (Hamamatsu, Japan) and Japan Laboratory Animals Inc. (Tokyo). SD-Tg (CAG-EGFP) rats and BALB/c Slc-nu/nu mice were from Nihon SLC Co. Ltd. (Hamamatsu, Japan). The donor rats were 34–56 days old (for anagen follicles), and the host rats and mice were 6–8 weeks of age. All animals were fed and watered *ad libitum*.

2.2. Mass culture of bulge cells

Vibrissa follicles were isolated from rats euthanized with chloroform and microdissected as described before (Kobayashi et al., 1993). Fragments containing only the bulge region were immersed in dispase solution (500 units/ml) and incubated for 30 min at 37 °C. The dermal sheath was teased away from the follicles, and the fragments were further incubated in a solution of 0.1% trypsin–0.02% ethylene diamine tetraacetic acid (EDTA) in calcium- and magnesium-free Dulbecco's PBS for 1 h at 37°C to completely dissociate the epithelial cells. These cells were centrifuged and re-suspended in a standard keratinocyte medium, a 3:1 mixture of Dulbecco modified Eagle's medium (DMEM), and Ham's F12 medium supplemented with 10% fetal bovine serum (Rheinwald and Green, 1975). The cells were then plated on a feeder layer consisted of 3T3 cells (Japanese Collection of Research Bioresources, Osaka, Japan), which had been lethally irradiated or treated with mitomycin C at 18 μg/ml for 4 h. The keratinocytes were cultured until semi-confluency and were passaged every week, being fed every 3 days. Human recombinant epidermal growth factor (EGF) was added at 10 ng/ml at the beginning of the first feed. All culture reagents were purchased from Gibco (Invitrogen Corp.; Carlsbad, CA), except for the mitomycin C (Sigma Chemical Co., St. Louis, MO) and the EGF (Invitrogen).

2.3. Cloning of bulge cells

Bulge cells were completely dissociated from vibrissa follicles as described, and transferred to a culture dish containing keratinocyte standard medium. Single cells were isolated with a Pasteur pipette by using an inverted microscope (Barrandon and Green, 1985) and individually cultured on a feeder layer of 3T3 cells lethally irradiated or treated with mitomycin C at 18 μg/ml.

2.4. Preparation of cell sheets and construction of recombinants

Bulge keratinocyte sheets were obtained from thermo-responsive dishes (CellSeed Inc., Tokyo, Japan). Mass cultured bulge cells at P2 and cloned bulge cells at P2 and P14 were plated on 3T3 feeder layers previously seeded on thermo-responsive dishes. After keratinocytes became confluent and formed a multilayered epithelium, approximately 10–14 days after plating, the culture medium was removed and the dishes were washed with DMEM. After incubation at 20 °C for 30 min, the multilayered keratinocyte sheets were peeled slowly from the edge of the dish with tweezers. The construction of recombinants (Fig. 1) was carried as described before (Xing and Kobayashi, 2001). Cell sheets were cut into 6 small pieces and a plate of sterilized silicon of 1 cm^2 was gently placed on the top of each epithelial fragment. The silicon plate with the cultured epithelium was then turned upside down so the basal layer side of the cell sheet faced up. Two to three DPs, freshly isolated from anagen vibrissa follicles, and sole dermis fragments were gently placed on the sheet and the peripheral cultured epithelium was gently wrapped back (represented in Fig. 1 by small arrows), so the DPs could be stably trapped between the tissues. Remaining pieces of the detached sheets were also fixed in neutral buffered formaldehyde for histological observations.

2.5. Construction of DP-upper follicle and DP-sole skin recombinants

To demonstrate that mechanically isolated DPs were devoid of matrix cells and consequently validate our tissue isolation technique and the results of induction experiments, DP-sole skin and DP-upper follicle recombinants containing DPs from EGFP-transgenic rats were used as control experiments. DP-upper follicle recombinants were prepared as described before (Oliver, 1966; Kobayashi and Nishimura, 1989). In brief, anagen vibrissa follicles isolated from donor rats were divided in two fragments by transection, and associated with a fresh DP at their amputated base. To prepare DP-sole skin recombinants, the glabrous region of sole skin fragments were treated with dispase (500 units/ml) for 30 min at 37 °C and rinsed with DMEM. The epidermis was partially detached from the dermis, creating a pocket where DPs were gently introduced.

2.6. Grafting

Rats were anesthetized by intramuscular injection of KETALAR® 50 (ketamine hydrochloride, 0.2–0.25 ml/6–8-week-old rats), the dorsal area of each rat was shaved and the required back skin was disinfected with 70% alcohol. A vertical incision was made in the back skin, a pocket was opened beneath it, where the recombinants were introduced onto the muscle fascia, with the dermis being in direct contact with the host rat hypodermis. The incision was closed with commercially available liquid adhesive. Nude mice were used as hosts for control grafts. DP-sole skin recombinants were transplanted as described above. DP-upper follicle recombinants were transplanted under the kidney capsule of nude mice as described before (Kobayashi and Nishimura, 1989).

2.7. Histology

The recombinants were harvested 3 weeks after transplantation, fixed in Bouin's solution or neutral buffered formaldehyde and embedded in paraffin. The sections (6 μm) were stained in a combination of Weigert's iron-hematoxylin, 1% Alcian blue and Curtis's Ponceau S solution.

2.8. Immunohistochemistry

Control grafts containing DPs isolated from EGFP-transgenic rats were fixed in 4% paraformaldehyde–PBS and embedded in paraffin. The sections (6 μm) were treated with rabbit anti-GFP serum (Molecular Probes Inc., Eugene, OR, USA) for 2 h at room

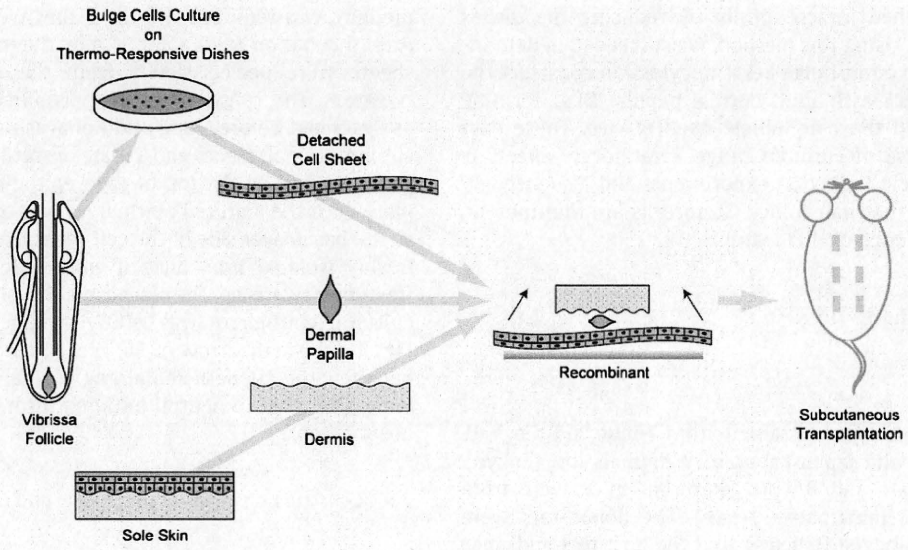

Fig. 1. Cultured keratinocyte sheets preparation and transplantation design. Bulge cells isolated from adult rat vibrissa follicles were plated in thermo-responsive dishes. After confluency, the dishes were incubated at 20 °C for 30 min, and the cells were harvested as a sheet and recombined with intact DPs and sole skin dermis, both also isolated from adult rats. The recombinants were placed in silicon sheets with the epidermis facing down, and then transplanted subcutaneously in the rat back skin.

temperature and the primary antibody was detected using the DAKO ENVISION kit and 3,3′-diaminobenzidine (DAB).

2.9. RT-PCR

To study the gene expression of specific markers in the cells used in the recombinants construction, total mRNAs were prepared from approximately 3×10^5 cells of mass cultured bulge cells at P2, and cloned bulge cells at P2 and P14. Total mRNAs were extracted with ISOGEN (Nippon Gene Co. Ltd.; Tokyo, Japan) and first-strand cDNAs were synthesized by using the Reverse Transcriptase XL (Takara Bio Inc.; Otsu, Japan). Reverse transcription PCR (RT-PCR) amplifications were performed using the following settings: 94 °C for 30 s, 55 °C for 30 s and 72 °C for 1 min; for 30 cycles. The primers were specific to the sequences for keratin 5 (krt5), 5′-GATCCATCTCTCCAGCGTGT-3′ and 5′-AACTCATTCTCTGCCGCTGT-3′; keratin 14 (krt14), 5′-AATGACCGCTGGCCTCCTA-3′ and 5′-TGGGCAGCCTCAGTTCTTG-3′; CD34, 5′-CACCAGAGCTATTCCCGAAA-3′ and 5′-TTCTGTGTCAGCCACCACAT-3′; S100A4, 5′-GAGGAGGCCCTGGATGTAAT-3′ and 5′-CTCACAGCCAACATGGAAGA-3′; S100A6, 5′-TCTAGCCCAGTGGTCAGTCA-3′ and 5′-CATCTCTGCCTTCCCATTTT-3′; Bmi-1, 5′-TGTGCGTTACTTGGAGACCA-3′ and 5′-TCATTCACCTCCTCCTTTGG-3′; and Zfp 145, 5′- AAAGCAGAGGACCTGGATGA-3′ and 5′-TCATGGCTGAGAGACCAAAA-3′.

3. Results

3.1. Bulge cell clones display stem cells characteristics in vitro

To prepare cultured epithelium sheets from a single bulge keratinocyte, 130 bulge cells were selected with a Pasteur pipette under an inverted microscope and individually cultured on 3T3 cell layers. After 1 week of culture, 27 clones were identified, representing a cloning efficiency of 20%. Eight clones were selected and grown to mass culture through 14 passages (P14), showing high proliferative ability, one of the stem cells characteristics. Prior to sheet preparation and construction of recombinants, RT-PCR was performed with mass cultured bulge keratinocytes at P2 and the eight selected cloned bulge keratinocytes at P2 and P14, in order to study the gene expression and characterize these cells. All samples expressed krt5 and krt14, epithelial basal layer cell markers also commonly found in the bulge region. The expression of well-established stem cell markers CD34 (Cotsarelis, 2006), S100A4 and S100A6 (Ito and Kizawa, 2001) were also confirmed. Bmi-1 and Zfp145, genes reported to contribute to the renewal and maintenance of stem cells (Park et al., 2003; Buaas et al., 2004), were also expressed in all types of the cultured bulge keratinocytes (Fig. 2, representative samples). Furthermore, krt14 expression was confirmed by immunohistochemistry in all cultured bulge cells and transplanted sheets (data not shown).

3.2. Transplantable bulge cell sheets can be harvested from thermo-responsive dishes

Mass cultured (P2) and cloned (P2 and P14) keratinocytes isolated from the bulge area of vibrissa hair follicles (Fig. 3A) were cultured for 10–14 days until they became confluent and formed a multilayered epithelium homogeneously over the surface of thermo-responsive dishes (Figs. 3B–D, representative samples). The dishes were then incubated at 20 °C for 30 min in order to detach the cells as a sheet. The sheets were intact, without holes or dissociated keratinocytes, being strong enough to be easily manipulated and transplanted onto the back skin of rats, a result that was never achieved by conventional enzymatic methods (data not shown). Histological observations revealed that the sheets were well organized, with a columnar layer of basophilic basal cells strongly stained by hematoxylin. Above the basal layer, stratified cells were observed and each sheet had at least a total of 3 cell layers (Figs. 3E–G, representative samples).

3.3. Cultured bulge cell sheets respond to DP signals in vivo

Cultured bulge sheets prepared with the use of thermo-responsive dishes were recombined with freshly isolated DPs and sole skin dermis for subcutaneous transplantation. A total of 16 grafts were prepared with bulge keratinocyte sheets and in all these samples regeneration of epidermis was observed (Table 1). The epidermal structure was similar to a normal one, with all its inherent layers; a single columnar layer of basal cells with large nuclei in a regular arrangement, a flattened spinous cell layer, a

granular layer, and a fully keratinized cornified layer (Fig. 4A). Sebaceous gland-like structures were also observed in all samples and always in a great number (Fig. 4B). Structures with a single layer of cuboidal cells deeply stained in the periphery of the acini, and with large cells containing light-stained cytoplasm located towards the center, resembled normal sebaceous glands (Fig. 4C). Epithelial cells surrounded the DP and formed a hair bulb in 11 (68.8%) of the transplanted recombinants. In these samples, the hair cuticle and the inner root sheath differentiation was confirmed by weak and strong staining with Curtis' Ponceau S solution, respectively (Figs. 4D, E). Through the observation of serial sections, further differentiation of the hair shaft was found in 2 samples (Fig. 4F), demonstrating that mature induced follicles were able to produce hair fibers *in vivo*.

Although cloned bulge cells showed high proliferative ability *in vitro*, expressed stem cells markers regardless the number of passages, and were successfully harvested as sheets from thermo-responsive polymers, none of the 8 clones selected regenerated the epidermis and sebaceous gland-like structures in the grafts. They also did not respond to DP signals when transplanted *in vivo*. Any remaining cells or keratinized structures were not observed in the graft site (data not shown).

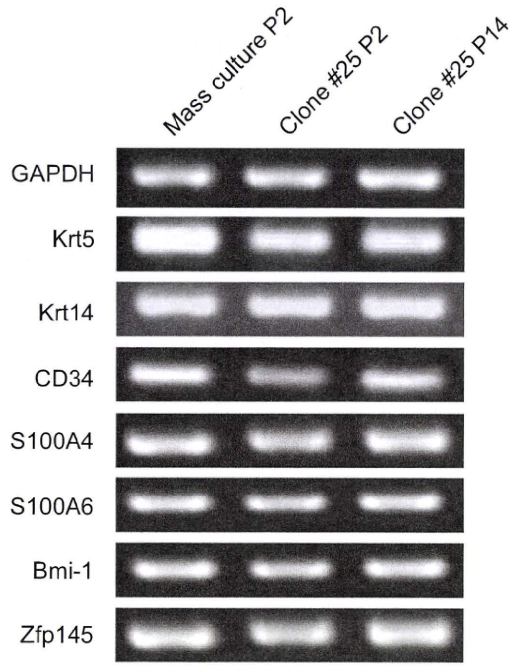

Fig. 2. Bulge cells express basal layer cells and stem cells markers *in vitro*. RT-PCR was performed with total mRNA extracted from freshly isolated bulge keratinocytes and cloned keratinocytes at P2 and P14. The expression of basal layer cells markers krt5 and krt14; stem cells markers CD34, S100A4 and S100A6; and genes reported to contribute to the renewal and maintenance of stem cells Bmi-1 and Zfp145 were confirmed in all types of bulge keratinocytes used in the preparation of cell sheets.

3.4. Control experiments

Control DP+keratinocyte epithelium recombinants containing DPs isolated from EGFP-transgenic rats were harvested 3 weeks after transplantation and analyzed using immunohistochemistry.

Table 1
Number of DP-cultured bulge keratinocytes recombinants containing the following types of structure.

Observed structures	Number of grafts (%)
Epidermis	16 (100)
Sebaceous gland	16 (100)
Hair matrix	11 (68.8)
Inner root sheath	11 (68.8)
Hair shaft	2 (12.5)
No follicular structures	2 (12.5)

Epidermis regeneration and sebaceous glands formation were observed in all grafts prepared from mass cultured bulge keratinocytes containing DPs. In 11 samples, hair matrix and IRS differentiation were confirmed, and in 2 samples the differentiation of hair shaft was also observed. In another 2 samples, follicular structures were not found regardless the epidermis regeneration and the presence of DP in the grafts.

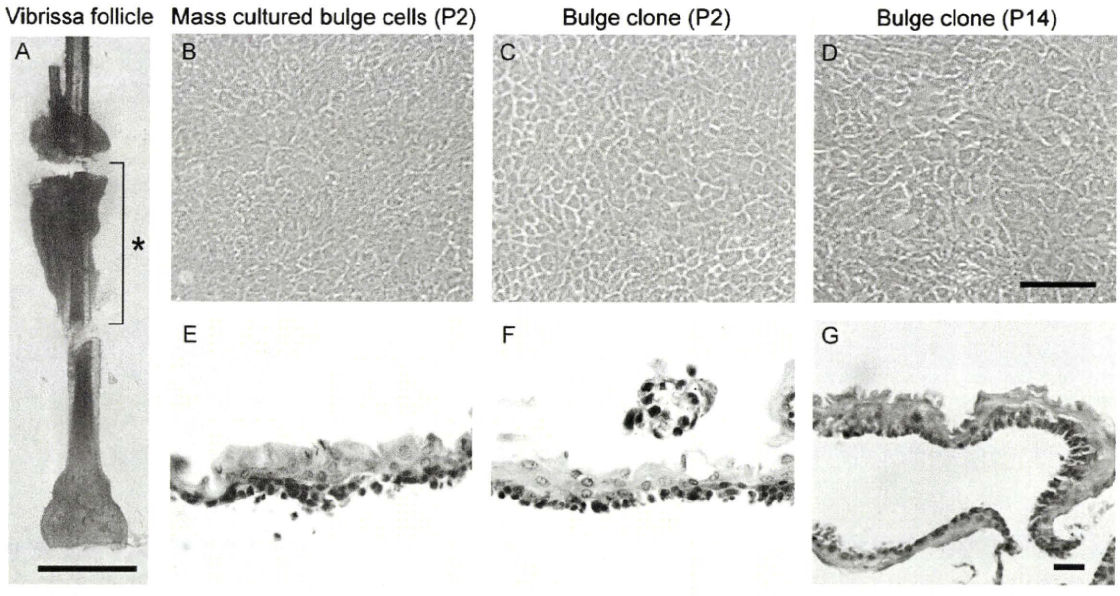

Fig. 3. Bulge keratinocytes culture and sheet preparation. (A) Keratinocytes were isolated from the bulge region of rat vibrissa follicles (asterisk), excluding the sebaceous gland in the upper part of the swelling. (B–D) Mass and cloned cells culture of bulge keratinocytes at confluency, prior to sheet preparation. (E–F) Histology of bulge keratinocytes sheets used in the transplantation experiments. The sheets were intact, without dissociated keratinocytes, and showed a well-organized basophilic layer of basal cells. Bars: 100 μm.

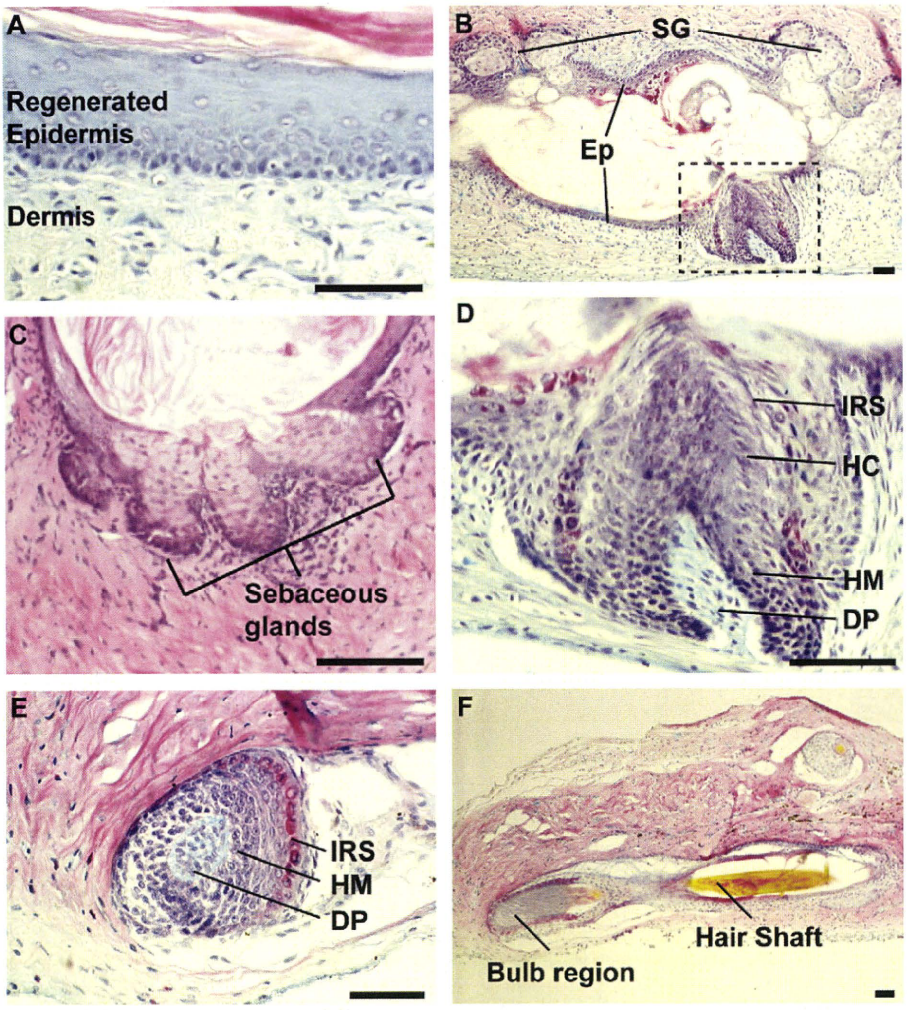

Fig. 4. Bulge keratinocytes respond to DP signals *in vivo*. (A) Epidermis regenerated from transplanted bulge keratinocytes sheets. (B) Epidermis (Ep) regeneration and sebaceous gland (SG) and a hair bulb-like structure (dotted line) formation in a representative sample. The sebaceous glands appear surrounding the epidermis in great number. (C) Magnification of sebaceous glands induced in bulge keratinocytes sheets, where a single layer of cuboidal cells enfolds larger cells with light-stained cytoplasm in the center, resembling normal ones. (D) Magnification of the hair bulb-like structure shown within dotted lines in (B). The epidermis surrounding the DP formed the hair matrix (HM) cells that further differentiated in the hair cuticle (HC) and the inner root sheath (IRS). (E) Another representative sample with an induced hair bulb-like structure where the follicular layers can be observed. (F) Serial section of (E), where the hair shaft differentiation was found 3 weeks after transplantation. Bars: 100 μm.

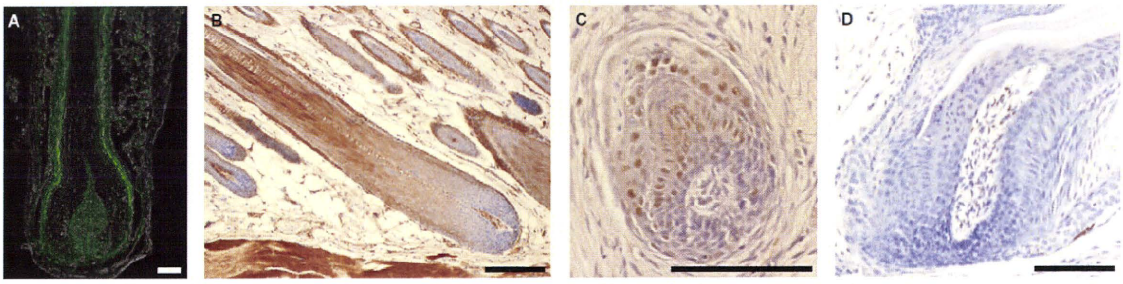

Fig. 5. Control experiments. (A) EGFP-transgenic mouse anagen vibrissa follicle. (B) Anti-GFP immunohistochemistry of EGFP-transgenic rat back skin. (C) Anti-GFP immunohistochemistry of hair follicle induced in DP-upper follicle recombinant containing DP isolated from EGFP-transgenic rat. (D) Anti-GFP immunohistochemistry of hair follicle induced in DP-sole skin recombinant containing DP isolated from EGFP-transgenic rat. Bars: 100 μm.

Since GFP expression is very weak in matrix cells of transgenic mice (Fig. 5A) and rats (Fig. 5B), their presence of small numbers of contaminating matrix cells in isolated DPs could not be directly detected by GFP expression. However, if small numbers of contaminating matrix cells were retained in mechanically isolated DPs and contributed to hair follicle formation, we hypothesized that their progeny would be recognized by GFP expression. Four hair bulbs regenerated from a total of 16 transplanted DP-upper follicle recombinants (Fig. 5C) and GFP-positive cells were found in 3 out of 4 of these regenerated hair bulbs, indicating the presence of contaminating matrix cells in 3 DPs. Only one successful hair follicle induction was obtained from a total of 15 DP-sole epidermis recombinants. GFP-positive cells were not found in this recombinant (Fig. 5D), suggesting that DPs were

devoid of matrix cells. The success rates of hair follicle induction in DP-sole epidermis recombinants (1/15) and hair bulb regeneration from DP upper follicle recombinants (3/16) were considerably low, whereas the rate of epithelial contamination was rather high (4/6 induced or regenerated follicles). However, observation of serial sections of these recombinants revealed that contaminating GFP-positive cells form only a small population of the induced or regenerated follicles (data not shown), meaning that most of the induced hair follicles were formed from the target keratinocyte epithelium. Taken together, these findings suggest that adult bulge epithelium is indeed capable of being induced by DP to form the entire hair follicle complex.

4. Discussion

Hair follicle stem cells have been isolated, characterized and applied for transplantation experiments in different studies. It has been reported that follicular structures are induced when bulge cells are mixed with non-adult mesenchymal components *in vivo* (Morris et al., 2004; Blanpain et al., 2004; Claudinot et al., 2005), but there is still no direct evidence for their multipotency and their ability to completely regenerate tissues *de novo* when recombined with adult tissues or cells. In this study, we addressed these questions by transplanting recombinants of cultured bulge keratinocytes sheets and adult rat vibrissa DPs.

Previous studies using adult rat sole keratinocytes have already demonstrated that cultured epithelium sheets can be useful tools in hair follicle induction experiments (Xing and Kobayashi, 2001; Miyashita et al., 2004). Since bulge cells cannot be harvested as a sheet by conventional enzymatic methods (data not shown), probably due to the lack of desmosomal components observed *in vivo* (Akiyama et al., 2004), thermo-responsive dishes were used to harvest intact bulge keratinocytes sheets and try a similar approach for hair follicle induction. Using thermo-responsive dishes, cell sheets can be harvested simply by reducing the temperature of the dishes. In contrast to those harvested by dispase treatment, these sheets are known to retain molecules like E-cadherin, laminin 5 and desmosomes intact (Yamato et al., 2001), and the use of these sheets proved to be functionally efficient in corneal reconstruction (Nishida et al., 2004a, b).

Bulge keratinocytes isolated from vibrissa follicles were cultured for 10–14 days, harvested as sheets and combined with adult rat vibrissa DPs. Recombinants were transplanted subcutaneously in the rat back skin and harvested 3 weeks after transplantation for histological observations. All samples were characterized by the presence of an organized epidermis and numerous sebaceous gland-like structures. Although hair follicle induction occurred with less efficiency, samples with differentiated hair cuticle, inner root sheath, and hair shaft were observed. These results show that cultured bulge keratinocytes can respond to adult DP signals *in vivo*, and directly demonstrate that bulge keratinocytes are multipotent. Studies which have used neonatal skin tissues or cells favored the analysis of an environment that was already organized and prepared to form skin appendages (Claudinot et al., 2005), or that was already engaged in this formation process (Blanpain et al., 2004; Morris et al., 2004). In the present model, cultured bulge cells reconstructed the skin structure and its appendages relying only on its multipotency and morphogenetic signals of DPs. Therefore, this model favors the analysis and comprehension of the true potential of adult hair follicle stem cells in a more direct way.

The DP, a cluster of specialized fibroblasts found in the base of the hair follicle, is known to play key roles in hair follicle development (Millar, 2002) and postnatal cyclic growth (Paus and Foitzik, 2004). The adult DP is also known to have hair follicle-inducing ability, as demonstrated by studies that have implanted DP cells into the upper half of vibrissa follicles (Oliver, 1966), or inserted them in the dermal–epidermal junction of glabrous skin (Oliver, 1970; Jahoda and Oliver, 1981; Reynolds and Jahoda, 1991, 1992; Jahoda, 1992; Osada et al., 2007). Whether the DP was the direct source of stimuli to induce the sebaceous gland-like structures is unknown in these reports. In the present experiments, sebaceous gland-like structures were observed with DP recombinants as shown in the results, but were not found without DP (control recombinants, data not shown). Consequently, the present finding suggests a new role for the DP as a source for sebaceous gland induction signals and this is also consistent with previous studies in which sebaceous gland formation eventually occurred when DP was present (Ferraris et al., 1997).

Although bulge stem cells are characterized by their slow cell cycling *in vivo*, they show high clonogenecity and proliferative capacity in culture (Cotsarelis et al., 1990; Kobayashi et al., 1993). Cloned bulge keratinocytes used in the preparation of sheets could be cultivated for over 14 passages, self-renewing for more than 150 doublings. The expression of well-established stem cells markers such as CD34 (Cotsarelis, 2006), S100A4 and S100A6 (Ito and Kizawa, 2001), and basal layer cells markers krt5 and krt14 was constantly observed during this period. Bmi-1 and Zfp145, genes reported to be important for the renewal of hematopoietic stem cells and germ cells, respectively (Park et al., 2003; Buaas et al., 2004), were also expressed *in vitro*. Taken together, these results demonstrate that the keratinocytes isolated were clonogenic stem cells of ORS origin with high proliferative ability and self-renewal capacity.

Despite the signs of stem cell identity *in vitro*, cloned bulge keratinocytes at P2 and P14 did not regenerate epidermis nor formed hair follicles or sebaceous glands *in vivo*. According to Claudinot et al. (2005) stem cells should be diploid to achieve successful engraftments. An anomaly in the chromosomes due to the long-term culture (P14) of cloned bulge keratinocytes could explain why follicular structures were not found in the transplanted recombinants. However, that would not apply to clones at P2 because such short-term culture would not be enough to give rise to anomalies in the chromosomes of all cells. The possibility that clones had transient amplifying (TA) cells can also be discarded because all the 27 cloned cells could be cultivated until P14, and it is plausible to think that TA cells should have their growth potential exhausted by this time. Our present explanation for the reason why cloned bulge keratinocytes failed to regenerate any follicular structures *in vivo* is in the polyclonal nature of hair follicles. Past studies that characterized induced hair follicles have shown that these structures are reconstituted from a minimum of two progenitor cells (Kamimura et al., 1997; Miyashita et al., 2004). Furthermore, the tracing of genetically marked cells revealed the presence of multiple classes of epidermal stem cells with restricted lineages (Ghazizadeh and Taichman, 2001). Assuming that hair follicles are polyclonal structures, a homogeneous population like the ones used in this study is not enough to give rise to all follicular structures. Claudinot et al. (2005) have demonstrated that progenitors of a single bulge keratinocyte can contribute to epidermis organization and give rise to hair follicles. This discrepancy in relation to our results might be due to the differences between the transplantation protocols used to induce hair follicles. It should be considered that in their transplantation model, transplanted bulge keratinocytes intermix with the host skin's cells that are already engaged in the process of hair follicle formation. In the present study, hair follicles were induced from a single cell source, the cultured epithelium, which had to reconstruct skin structures *de novo*. Transplantation experiments to be performed with keratinocytes sheets containing progenitors

of two or more clones could elucidate the differences between the mixed- and single-cell progenitors population.

Two different types of recombinants containing DPs isolated from EGFP-transgenic rats were used as control experiments to demonstrate that mechanically isolated DPs are devoid of matrix cells. The results from these experiments suggest that the purity of DPs is questionable, as some of them might carry matrix cells that eventually contribute to hair follicle formation. The presence of matrix cells attached to the DP represents a limitation of the isolation technique itself, which relies on mechanical microdissection. A pure population of DP cells could be obtained *in vitro*. However, such cells could be considered an artifact of the culture system, which basically relies on growth factors and would not be representative of the actual features of the original tissue (Jahoda and Oliver, 1981; Inamatsu et al., 1998; Osada et al., 2007). By contrast, mechanically dissected DPs allow the direct study of induction capacity in intact adult tissues. Although contamination of matrix cells may be inevitable during isolation of DPs, their contribution to follicle formation would not be much.

In conclusion, the present study demonstrates for the first time that cultured bulge keratinocytes sheets can be obtained by using thermo-responsive dishes. Using these sheets, we also succeeded in giving direct evidences of bulge stem cells multipotency; bulge keratinocytes could regenerate epidermis and form sebaceous glands and hair follicles when interacted with adult DPs *in vivo*. This model not only facilitates basic studies on adult tissue stem cells, but is also a promising tool for clinical application, considering that adult human cells are of easier accessibility than their embryonic counterparts. Furthermore, the cultured bulge keratinocytes sheets could also be applied in the establishment of an *in vitro* system that reproduces the hair follicle development. Such a system would be useful to the analysis and comprehension of this complex process. Due to the bulge stem cells multipotency, the sheets would facilitate hair follicle formation, and thanks to their arrangement, the multilayering of cells would also contribute to faster formation of skin equivalents *in vitro*.

Acknowledgments

This work was supported by grants from Suzuken Memorial Foundation, the Center of Excellence (COE) Program for the 21st Century, the High-Tech Research Center Program, and the Formation of Innovation Center for Fusion of Advanced Technologies in the Special Coordination Funds for Promoting Science and Technology, from the Ministry of Education, Culture, Sports, Science and Technology (MEXT), Japan. The authors thank Dr. Tomohisa Hirobe (National Institute of Radiological Sciences, Japan) for the gamma ray irradiation of 3T3 cells, Dr. Asako Terasaki (Chiba University, Japan) for the cooperation during the performance of control experiments and Dr. Susan Willi Monnerat for the proofreading of this manuscript.

References

Akiyama, M., Sawamura, D., Shimizu, H., Matsuo, I., 2004. Remodeling of desmosomal and hemidesmosomal adhesion systems during human hair follicle development. J. Dermatol. Sci. 35, 154–157.

Barrandon, Y., Green, H., 1985. Cell size as a determinant of the clone-forming ability of human keratinocytes. Proc. Natl. Acad. Sci. USA 82, 5390–5394.

Blanpain, C., Lowry, W.E., Geoghegan, A., Polak, L., Fuchs, E., 2004. Self-renewal, multipotency, and the existence of two cell populations within an epithelial stem cell niche. Cell 118, 635–648.

Buaas, F.W., Kirsh, A.L., Sharma, M., McLean, D.J., Morris, J.L., Griswold, M.D., de Rooij, D.G., Braun, R.E., 2004. Plzf is required in adult male germ cells for stem cell self-renewal. Nat. Genet. 36, 647–652.

Claudinot, S., Nicolas, M., Oshima, H., Rochat, A., Barrandon, Y., 2005. Long-term renewal of hair follicles from clonogenic multipotent stem cells. Proc. Natl. Acad. Sci. USA 102, 14677–14682.

Cotsarelis, G., 2006. Epithelial stem cells: a folliculocentric view. J. Invest. Dermatol. 126, 1459–1468.

Cotsarelis, G., Sun, T.T., Lavker, R.M., 1990. Label-retaining cells reside in the bulge area of pilosebaceous unit: implications for follicular stem cells, hair cycle, and skin carcinogenesis. Cell 61, 1329–1337.

Ferraris, C., Bernard, B.A., Dhouailly, D., 1997. Adult epidermal keratinocytes are endowed with pilosebaceous forming abilities. Int. J. Dev. Biol. 41, 491–498.

Ghazizadeh, S., Taichman, L.B., 2001. Multiple classes of stem cells in cutaneous epithelium: a lineage analysis of adult mouse skin. EMBO J. 20, 1215–1222.

Inamatsu, M., Matsuzaki, T., Iwanari, H., Yoshizato, K., 1998. Establishment of rat dermal papilla cell lines that sustain the potency to induce hair follicles from afollicular skin. J. Invest. Dermatol. 111, 767–775.

Ito, M., Kizawa, K., 2001. Expression of calcium-binding S100 proteins A4 and A6 in regions of the epithelial sac associated with the onset of hair follicle regeneration. J. Invest. Dermatol. 116, 956–963.

Jahoda, C.A.B., 1992. Induction of follicle formation and hair growth by vibrissal dermal papillae implanted into rat ear wounds: vibrissa-type fibres are specified. Development 115, 1103–1109.

Jahoda, C., Oliver, R.F., 1981. The growth of vibrissa dermal papilla cells *in vitro*. Br. J. Dermatol. 105, 623–627.

Kamimura, J., Lee, D., Baden, H.P., Brissette, J., Dotto, G.P., 1997. Primary mouse keratinocyte cultures contain hair follicle progenitor cells with multiple differentiation potential. J. Invest. Dermatol. 109, 534–540.

Kobayashi, K., Nishimura, E., 1989. Ectopic growth of mouse whiskers from implanted lengths of plucked vibrissa follicles. J. Invest. Dermatol. 92, 278–282.

Kobayashi, K., Rochat, A., Barrandon, Y., 1993. Segregation of keratinocyte colony-forming cells in the bulge of the rat vibrissa. Proc. Natl. Acad. Sci. USA 90, 7391–7395.

Millar, S.E., 2002. Molecular mechanisms regulating hair follicle development. J. Invest. Dermatol. 118, 216–225.

Miyashita, H., Hakamata, Y., Kobayashi, E., Kobayashi, K., 2004. Characterization of hair follicles induced in implanted, cultured rat keratinocyte sheets. Exp. Dermatol. 13, 491–498.

Morris, R.J., Liu, Y., Marles, L., Yang, Z., Trempus, C., Li, S., Lin, J.S., Sawicki, J.A., Cotsarelis, G., 2004. Capturing and profiling adult hair follicle stem cells. Nat. Biotechnol. 22, 411–417.

Nishida, K., Yamato, M., Hayashida, Y., Watanabe, K., Maeda, N., Watanabe, H., Yamamoto, K., Nagai, S., Kikuchi, A., Tano, Y., Okano, T., 2004a. Functional bioengineered corneal epithelial sheet grafts from corneal stem cells expanded ex vivo on a temperature-responsive cell culture surface. Transplantation 77, 379–385.

Nishida, K., Yamato, M., Hayashida, Y., Watanabe, K., Yamamoto, K., Adachi, E., Nagai, S., Kikuchi, A., Maeda, N., Watanabe, H., Okano, T., Tano, Y., 2004b. Corneal reconstruction with tissue-engineered cell sheets composed of autologous oral mucosal epithelium. N. Engl. J. Med. 351, 1187–1196.

Oliver, R.F., 1966. Histological studies of whisker regeneration in the hooded rat. J. Embryol. Exp. Morphol. 16, 231–244.

Oliver, R.F., 1970. The induction of hair follicle formation in the adult hooded rat by vibrissa dermal papillae. J. Embryol. Exp. Morphol. 23, 219–236.

Osada, A., Iwabuchi, T., Kishimoto, J., Hamazaki, T.S., Okochi, H., 2007. Long-term culture of mouse vibrissal dermal papilla cells and *de novo* hair follicle induction. Tissue Eng. 13, 975–982.

Oshima, H., Rochat, A., Kedzia, C., Kobayashi, K., Barrandon, Y., 2001. Morphogenesis and renewal of hair follicles from adult multipotent stem cells. Cell 104, 233–245.

Park, I.K., Qian, D., Kiel, M., Becker, M.W., Pihalja, M., Weissman, I.L., Morrison, S.J., Clarke, M.F., 2003. Bmi-1 is required for maintenance of adult self-renewing haematopoietic stem cells. Nature 423, 302–305.

Paus, R., Foitzik, K., 2004. In search of the "hair cycle clock": a guided tour. Differentiation 72, 489–511.

Reynolds, A.J., Jahoda, C.A., 1991. Inductive properties of hair follicle cells. Ann. NY Acad. Sci. 642, 226–241 [discussion 241–2].

Reynolds, A.J., Jahoda, C.A., 1992. Cultured dermal papilla cells induce follicle formation and hair growth by transdifferentiation of an adult epidermis. Development 115, 587–593.

Rheinwald, J.G., Green, H., 1975. Serial cultivation of strains of human epidermal keratinocytes: the formation of keratinizing colonies from single cells. Cell 6, 331–343.

Taylor, G., Lehrer, M.S., Jensen, P.J., Sun, T.T., Lavker, R.M., 2000. Involvement of follicular stem cells in forming not only the follicle but also the epidermis. Cell 102, 451–461.

Xing, L., Kobayashi, K., 2001. Ability of transplanted cultured epithelium to respond to dermal papillae. Tissue Eng. 7, 535–544.

Yamato, M., Utsumi, M., Kushida, A., Konno, C., Kikuchi, A., Okano, T., 2001. Thermo-responsive culture dishes allow the intact harvest of multilayered keratinocyte sheets without dispase by reducing temperature. Tissue Eng. 7, 473–480.

Impaired Myocardium Regeneration With Skeletal Cell Sheets—A Preclinical Trial for Tissue-Engineered Regeneration Therapy

Shigeru Miyagawa,[1] Atsuhiro Saito,[2] Taichi Sakaguchi,[1] Yasushi Yoshikawa,[1] Takashi Yamauchi,[1] Yukiko Imanishi,[1] Naomasa Kawaguchi,[3] Noboru Teramoto,[4] Nariaki Matsuura,[3] Hidehiro Iida,[4] Tatsuya Shimizu,[5] Teruo Okano,[5] and Yoshiki Sawa[1,6]

Background. We hypothesized that autologous skeletal cell (SC) sheets regenerate the infract myocardium in porcine heart as a preclinical trial.

Methods and Results. The impaired heart was created by implantation of ameroid constrictor on left anterior descending for 4 weeks. SCs isolated from leg muscle were cultured and detached from the temperature-responsive domain-coated dishes as single monolayer cell sheet at 20°C. The following therapies were conducted: SC sheets (SC group, n=5); sham (C group n=5). Echocardiography demonstrated that cardiac performance was significantly improved in the SC group 3 and 6 months after operation (fractional area shortening, 3 months; SC vs. C=49.5±2.8 vs. 24.6±2.0%, $P<0.05$) and left ventricle dilatation was well attenuated in the SC group. Color kinesis index showed that distressed regional diastolic and systolic function in infarcted anterior wall was significantly recovered (SC vs. C=57.4±8.6 vs. 30.2±4.7%, $P<0.05$, diastolic: 58.5±4.5 vs. 35.4±6.6%, $P<0.05$, systolic). Factor VIII immunostains demonstrated that vascular density was significantly higher in the SC group than the C group. And % fibrosis and cell diameter were significantly lower in the SC group. And hematoxylin-eosin staining depicted that skeletal origin cells and well-developed-layered smooth muscle cells were detected in the implanted area. Positron emission tomography showed better myocardial perfusion and more viable myocardial tissue in the distressed myocardium receiving SC sheets compared with the myocardium receiving no sheets.

Conclusions. SC sheet implantation improved cardiac function by attenuating the cardiac remodeling in the porcine ischemic myocardium, suggesting a promising strategy for myocardial regeneration therapy in the impaired myocardium.

Keywords: Cells, Heart failure, Myocardial infarction, Tissue, Transplantation.

(*Transplantation* 2010;90: 364–372)

Despite the recent remarkable progress in medical and surgical treatments for heart failure, end-stage heart failure has been still a major cause of death worldwide. After myocardial infarction, the myocardium is capable of a limited regenerative capacity and no medication or procedure used clinically has shown efficacy in regenerating myocardial scar tissue with functioning tissue. Thus, there is a need for new therapeutics to regenerate damaged myocardium.

Recent developments in tissue engineering show promise for the creation of functional cardiac tissues without the need for biodegradable alternatives for the extracellular matrix (*1*). And we reported that cardiomyocyte sheets have been developed by using temperature-responsive culture dishes and these sheets survived in the back of nude rats and showed a spontaneous contraction over a long period of time (*2*). Recent reports suggested that cardiomyocyte sheets integrated with the impaired myocardium and improved cardiac performance in a rat model of ischemic myocardium (*3*).

This work was supported by a Grant-in-Aid for Scientific Research in Japan.

[1] Division of Cardiovascular Surgery, Department of Surgery, Faculty of Medicine, Osaka University Graduate School of Medicine, Suita, Osaka, Japan.

[2] Medical Center for Translational Research, Osaka University Hospital, Osaka, Japan.

[3] Department of Pathology, School of Allied Health Science, Faculty of Medicine, Osaka University Graduate School of Medicine, Suita, Osaka, Japan.

[4] Department of Investigative Radiology, National Cardiovascular Center Research Institute, Tokyo, Japan.

[5] Tokyo Women's Medical University Institute of Advanced Biomedical Engineering and Science, Tokyo, Japan.

[6] Address correspondence to: Yoshiki Sawa, M.D., Department of Cardiovascular Surgery, Osaka University Graduate School of Medicine, 2-2 Yamada-oka, Suita, Osaka 565-0871, Japan.
E-mail: sawa@surg1.med.osaka-u.ac.jp

S.M. participated in the writing of the paper; A.S. participated in research design; T.S. and Y.Y. participated in data analysis; T.Y., Y.I., N.K., and N.T. participated in the performance of research; N.M., H.I., T.S., T.O., and Y.S. participated in research design.

Received 15 December 2009. Revision requested 2 January 2010.
Accepted 6 May 2010.
Copyright © 2010 by Lippincott Williams & Wilkins
ISSN 0041-1337/10/9004-364
DOI: 10.1097/TP.0b013e3181e6f201

Copyright © Lippincott Williams & Wilkins. Unauthorized reproduction of this article is prohibited.

And more recently, in the aim of clinical application, nonligature implantation of skeletal myoblast sheet regenerated the damaged myocardium and improved global cardiac function by attenuating the cardiac remodeling in the rat ligation model (*4*) and dilated cardiomyopathy hamster model (*5*). This cell delivery system by using cell sheets implantation showed better restoration of damaged myocardium compared with needle injection (*4*, *5*). Moreover, grafting of skeletal myoblast sheets attenuated cardiac remodeling and improved cardiac performance in pacing-induced canine heart failure model (*6*).

Given this body of evidence, we hypothesized that the autologous skeletal cell (SC) sheet implantation might remodel the chronic heart failure caused by ischemic injury.

Therefore, this preclinical study using Swine model was designed to test therapeutic effectiveness.

MATERIALS AND METHODS

Myocardial Infarction Model

"Principles of Laboratory Animal Care" formulated by the National Society for Medical Research and the "Guide for the Care and Use of Laboratory Animals" prepared by the Institute of Laboratory Animal Resource and published by the National Institutes of Health (NIH Publication No. 86-23, revised 1985). This animal experiment was approved by the Animal Care Committee of Osaka university graduate school of medicine. We induced acute myocardial infarction of 10 swine (20 kg, KEARI, Japan) by the following method. Swine were preanesthetized by intramuscular injection of ketamine hydrochloride 20 mg/kg (Ketalar, Sankyo, Japan) and xylazine 2 mg/kg (Seractar, Bayer). Animals were positioned spine and a 22-gauge indwelling needle (Surflo F&F, Terumo, Tokyo, Japan) was inserted in the central vein of the auricle. A three-way cock (Terufusion TS-TR2K, Terumo, Tokyo, Japan) was attached to the external cylinder of the indwelling needle, and an extension tube was connected for continuous anesthetic injection. The animals were intubated with an endotracheal cannula (6 Fr, Sheridan) using a pharyngoscope and then connected to an artificial respirator (Harvard, USA) by the cannula. Artificial respiration was implemented at a stroke volume of 200 to 300 mL/stroke and a stroke frequency of 20/min. The animals were continuously drip injected with propofol 6 mg/kg/hr (Diprivan, AstraZeneca) and vecuronium bromide 0.05 mg/kg/hr (Musculux, Sankyo Yell Yakuhin Co., Ltd., Japan) using a syringe pump (Terufusion TE-3310N, Terumo, Japan). The animal was then fixed in a recumbent position, so that the left thorax was exposed, and the outer layer of skin and muscles between the third and fourth ribs were dissected. After confirming the cutting into the thoracic cavity, the distance between the third and fourth ribs was widened with a rib spreader to allow a direct view of the left auricle and the LAD coronary artery. The pericardium was dissected along the LAD from the upper part of the left auricle (~6 cm) to expose the myocardium around the LAD. LAD on the proximal side below the left auricle from the myocardium was exfoliated for approximately 1 cm, and then a small amount of lidocaine hydrochloride jelly (Xylocaine jelly, AstraZeneca) was applied to allow for anesthetizing the area. An ameroid constrictor (COR-2.50-SS, Research Instruments) was then fit using No. 1 or 2 suture. The chest cavity was closed to end the procedures. The animals were randomly divided into two treatment groups: the first received autologous SC sheet implantation (SC group, n=5). For control, we have performed sham operation (C group, n=5).

Preparation of Skeletal Cell Sheets for Grafting

One week after implantation of ameroid constrictor on LAD, skeletal muscle weighing approximately 5 g was removed from the pretibial region with the porcine under general anesthesia. Following the addition of trypsin-ethylenediaminetetraacetic acid (Gibco, Grand Island, NY), excessive connective tissue was carefully removed to minimize the content of contaminating fibroblasts, and the muscle tissue was minced until the fine pieces formed a homogeneous mass. The specimens were then incubated at 37°C in shaker bath with 0.5% type 1 collagenase (Gibco) in Dulbecco's modified Eagle's medium (Gibco). After brief placement, the fluid was collected, and the same volume of culture medium, SkBM (Cambrex, Walkersville, MD) supplemented with fetal bovine serum (Thermo Trace, Melbourne, Australia), was added to halt the enzymatic digestion process. The cells were collected by centrifugation, and the putative SCs were seeded into 150 cm^2 polystyrene flasks after removal of fibroblasts by sedimentation for a few hours and cultured in SkBM at 37°C. During the culture process, we maintained cell densities at less than 70% confluence by carrying out passaging of cells for one time to prevent SCs from premature differentiation and fusion process resulting in myotubes formation. When the cells become approximately 70% confluent after 10 to 11 days cultivation, the cells were dissociated from the flasks with trypsin-ethylenediaminetetraacetic acid and reincubated on 100 mm temperature-responsive culture dishes (Cellseed, Tokyo, Japan) at 37°C with the cell numbers adjusted to 1×10^7 per dish. More than 90% of these cells were desmin positive (Fig. 1). After 4 days, the dishes were removed to refrigerator set at 20°C, and left there for approximately 30 min. During that time, the SC sheets detached spontaneously from the surfaces. Each sheet had a diameter of 30 to 40 mm and consisted of layers of SCs; the sheets were approximately 100-μm thick in cross-sectional views (Fig. 1). Approximately 10 sheets were obtained from the 5 g of skeletal muscle.

Implantation of Skeletal Cell Sheets

Autologous SC sheet implantation was performed in the swine 4 weeks after LAD ligation. Swine were anesthetized as mentioned above. The swine were exposed through the sternum. The infarct area was identified visually on the basis of surface scarring and abnormal wall motion. In the SC group, we implanted 10 SC sheets into the infarcted myocardium. The control group was treated similarly but received no SC sheets. Because pilling up four or more sheets caused the central necrosis of the myoblasts presumably because the lack of in oxygen supply, we decided to pile two or three layers of the SC sheet over the broad surface of the impaired heart.

Measurement of Cardiac Function

Swine were anesthetized as mentioned above. Cardiac ultrasonography was performed with a commercially available echocardiograph, SONOS 5500 (PHILIPS Electronics, Tokyo, Japan). A 3-MHz annular array transducer was placed on a layer of acoustic coupling gel that was applied to the left hemithorax. Swine were examined in a shallow left lateral decubitus position. The heart was first imaged in the two-dimensional mode in short-axis views at the level of the largest left ventricle (LV) diameter. The calculation of the LV volume was based on the LV short-axis area using AQ system (*7*). And fractional area shortening (FAS) of the LV diastolic was calculated as follows:

$$\text{FAS (\%)} = [(\text{LVend-diastolic area} - \text{LV end-systolic area [ESA]})/\text{LV end-diastolic area}] \times 100$$

These data are presented as the average of measurements of two or three selected beats.

Quantification of Regional Diastolic and Systolic Function by Color Kinesis

Diastolic CK images were obtained using a commercially available ultrasound system (SONOS 5500, Philips Medical Systems) from the LV midpapillary short-axis view for the determination of wall motion asynchrony as previously reported (*8*). CK examined every image pixel within the region of interest, which was drawn around the LV cavity, classifying it as blood or tissue based on integrated backscatter data. During diastole, each pixel was tracked into the next frame, and pixel transitions from endocardium to blood were detected and interpreted as diastolic endocardial motions. These pixel transitions were encoded using a color hue specific to each consecutive video frame, so that each color represents the excursion of that segment during a 33-ms period of time. The sites of regional LV diastolic wall motion or regions of interest were set on the basis of standard segmentation models: anterior, lateral, posterior, inferior, anteroseptal wall. The CK diastolic index was defined as the LV segmental filling fraction

Copyright © Lippincott Williams & Wilkins. Unauthorized reproduction of this article is prohibited.

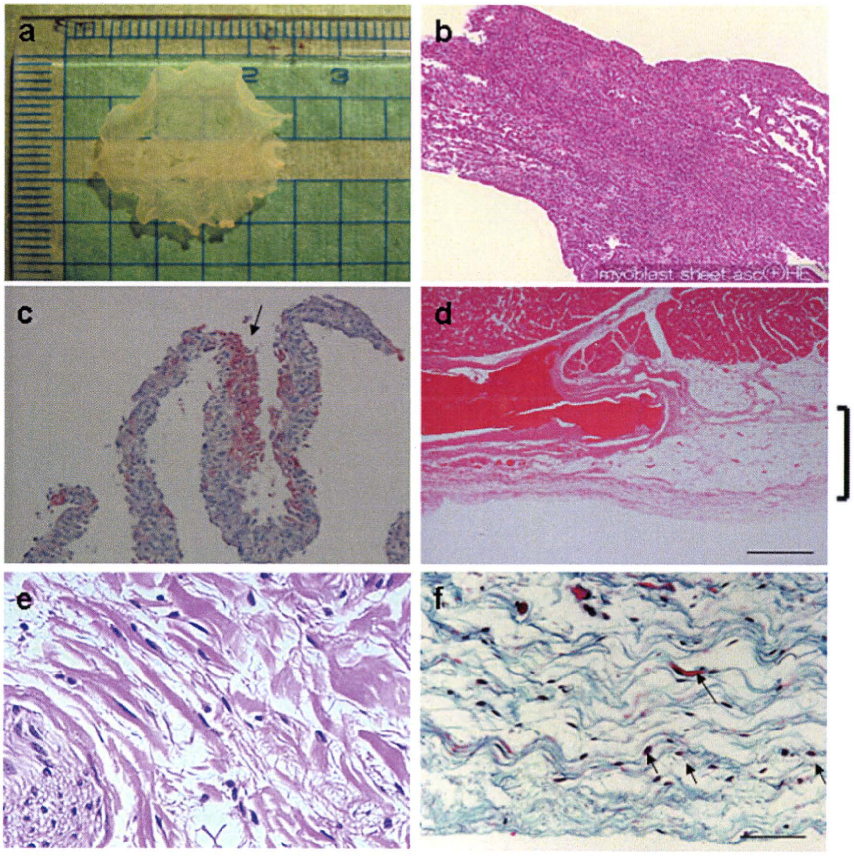

FIGURE 1. Histological characteristics of skeletal cell (SC) sheet. (a) SC sheet detached from the Poly (*N*-isopropylacrylamide)-grafted polystyrene by lowering the temperature. Its size is approximately 3 cm×2 cm^2. (b) Hematoxylin-eosin (H&E) stain; cross-sectional views of SC sheet in vitro. SC sheet demonstrates homogeneous heart-like tissue. (c) Not so many smooth muscle cells were detected in the SC sheets. The *arrow* indicates the smooth muscle cells in the SC sheet. (d) H&E stain revealed that SC sheets attached on the surface of epicardium. *Left square bracket* indicates implanted SC sheets. (e) Oval-shaped cells that showed positive for eosin in cytoplasm were detected in the SC group microscopically in some layers over epicardium. (f) Elastica Masson Goldner showed that oval-shaped cells that supposed to origin from skeletal tissue exist in the transplantation site. *Arrows* indicate oval-shaped cells that suppose to be originated form skeletal tissue.

during the first 30% of the diastolic filling time (LV segmental cavity area expansion during the first 30% of diastole, divided by the segmental end-diastolic LV cavity area expansion, expressed as a percentage). We introduced the use of color kinesis method that displays endocardial motion in real time to evaluate the regional systolic function (*8*).

Histopathology

LV myocardium specimens were obtained 6 months after the SC sheet implantation. Each specimen was fixed with 10% buffered formalin and embedded in paraffin. A few serial sections were prepared from each specimen and stained with hematoxylin-eosin (H&E) stain and elastica Masson-Goldner for histological examination or with Masson's trichrome stain to assess the collagen content.

To label vascular endothelial cells so that the blood vessels could be counted, immunohistochemical staining of factor VIII-related antigen was performed according to a modified protocol. Frozen sections were fixed with a 2% paraformaldehyde solution in phosphate-buffered saline (PBS) for 5 min at room temperature, immersed in methanol with 3% hydrogen peroxide for 15 min, then washed with PBS. The samples were covered with bovine serum albumin solution (DAKO LSAB Kit DAKO CORPORATION, Denmark) for 10 min to block nonspecific reactions. The specimens were incubated overnight with an Enhanced Polymer One-Step Staining (EPOS)-conjugated antibody against factor VIII-related antigen coupled with horseradish peroxidase (DAKO EPOS Anti-Human Von Wille brand Factor/HRP, DAKO, Denmark). After the samples were washed with PBS, they were immersed in diaminobenzidine solution (0.3 mg/mL diaminobenzidine in PBS) to obtain positive staining. Ten different fields at 200× magnification were randomly selected, and the number of the stained vascular endothelial cells in each field was counted under a light microscope. The result was expressed as the number of blood vessels per square millimeter.

The following antibodies against smooth muscle cells and skeletal myosin (slow) were used to evaluate the existence of SCs: primary antibodies, anti-smooth muscle actin (clone 1A4, DAKO) antiskeletal myosin (slow) (clone NOQ7.5.4D, Sigma); secondary antibodies, anti-mouse Ig biotinylate (DAKO).

Picro-sirius red staining for the assessment of myocardial fibrosis or periodic acid-Schiff staining for that of cardiomyocyte hypertrophy was performed as described (*9*).

Positron Emission Tomography Procedure

We performed positron emission tomography (PET) studies on pigs which were transplanted SC sheets and control by using ^{15}0-water and ^{18}F-FDG. The pigs were anesthetized by the introduction of pentobarbital followed by continuous inhalation of propofol (4 mg/kg/hr) and were placed supine on the bed of the scanner. PET was performed using a HEADTOME-III tomograph (Shimadzu, Kyoto, Japan) and data were analyzed as described elsewhere (*10*).

Holter Electrocardiography

To evaluate arrhythmia we used Holter electrocardiography (ECG) for 24 hours. We checked arrhythmia by checking the number of ventricular premature beat after SC sheet implantation in myocardial infarction porcine (n=3).

Data Analysis

Data are expressed as means ± SEM and subjected to multiple analysis of variance (ANOVA) using the StatView 5.0 program (Abacus Concepts, Berkeley, CA). Echocardiographic data were first analyzed by two-way repeated measurement ANOVA for differences across the whole time course, and one-way ANOVA with the Tukey-Kramer posthoc test was used to verify the significant for the specific comparison at each time point. To assess the significance of the differences between individual groups concerning other numeral data, statistical evaluation was performed with an unpaired *t* test. Statistical significance was determined as having a *P* value less than 0.05.

Copyright © Lippincott Williams & Wilkins. Unauthorized reproduction of this article is prohibited.

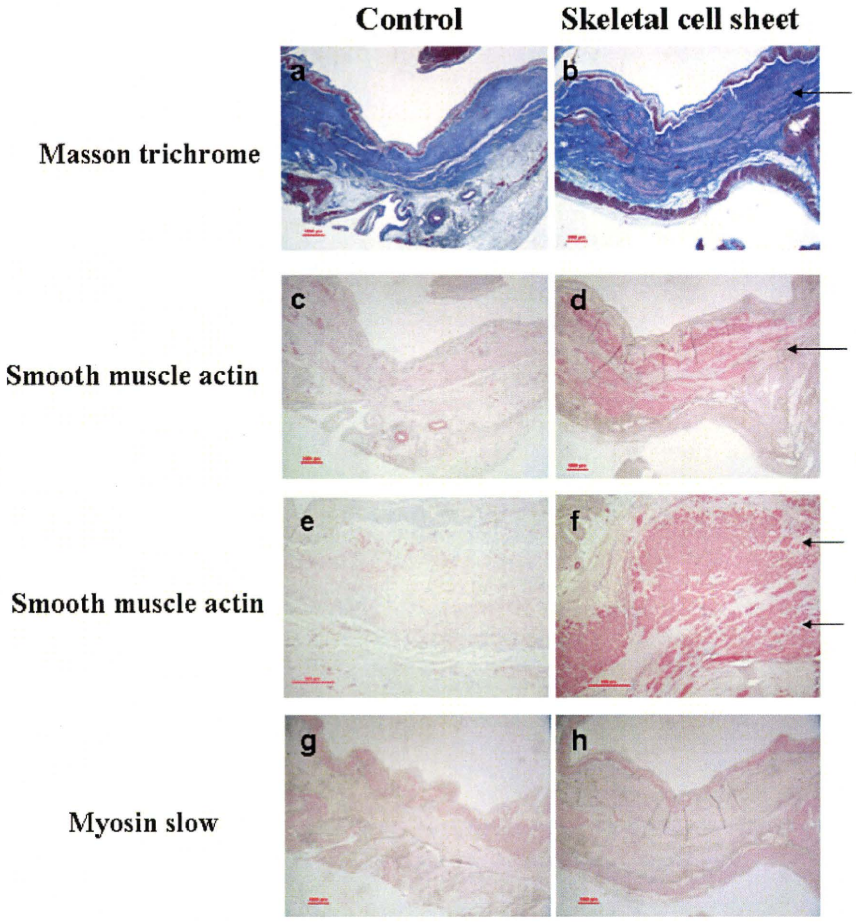

FIGURE 2. The detection of a large quantity of skeletal cells (SCs) in the center of the scar. (a and b) Masson trichrome staining reveals that some layered muscles are detected in the center of the scar in the SC sheet transplantation group, whereas not in the control. (c–f) Smooth muscle actin staining demonstrated that well-developed smooth muscle cells occupied in the center of the scar in the SC sheet transplantation group, whereas only smooth muscle cells which are formed vasculature are detected in the control. (g and h) Slow-type myosin staining showed that no positive cells exist in the center of the scar. This means that SCs which are detected in the center of the scar are not the residual myocyte after infarction.

RESULTS

Characteristics of Myoblast Sheet

We obtained monolayered myoblast sheets by lowering the temperature, which released them from the Poly(*N*-isopropylacrylamide)-grafted polystyrene. Its size is approximately 3 cm×2 cm^2 (Fig. 1a). H&E staining demonstrated that SC sheet contained a lot of SCs and SC sheets had an appearance of homogenous tissue, which thickness of one SC sheet was approximately 100 μm (Fig. 1b). Some smooth muscle cells are detected in the SC sheets, but those cells are not majority (Fig. 1c).

Histological Assessment

H&E staining demonstrated that transplanted SC sheets were attached in the epicardium (Fig. 1d) and oval-shaped cell that showed positive for eosin in cytoplasm were detected in the SC group microscopically in some layers over epicardium (Fig. 1e). Elastica Masson-Goldner showed that oval-shaped cells that supposed to origin from skeletal tissue exist in the transplantation site (Fig. 1f). These cells were not seen in the control group. And the SC group demonstrated decrease in the cross-sectional LV area compared with the C groups (Fig. 2a). Masson's trichrome staining showed that clustered SCs were detected in the center of the scar, whereas clustered SCs were not detected in the C group (Fig. 2a, b). Many clusters of well-developed smooth muscle cells exist in the center of the whole scar in the SC group, whereas in the C group, smooth muscle cells which formed vasculature exist in the scar (Fig. 2c–f). Although slow-type myosin-positive cells exist only on the endocardium and epicardium, those cells were not detected in the center of scar (Fig. 2g,h). So these figures depict that the skeletal muscle cells that exist in the center of the scar is not residual myocyte after infarction.

Quantification of Histopathology

In the SC group, vascular density was found to be significantly higher than in the C groups (SC vs. C=217.1±30.2 vs. 114.2±18.2 /field; $P<0.05$) (Fig. 3b).

Picro-sirius red staining demonstrated that % fibrosis was significantly reduced in the SC group compared with the C group (SC vs. C=1.6±0.2 vs. 3.1±0.3%; $P<0.05$) (Fig. 3b). Periodic acid-Schiff staining showed that cell diameter was significantly shorter in the SC group than the C group (SC vs. C=10.7±0.3 vs. 18.3±1.4 μm; $P<0.05$) (Fig. 3b).

These histological findings were universally identified in the native myocardial tissue without distinction of distance from the grafted region.

Functional Assessment of the Infarcted Myocardium

The FAS and LV end-ESA scores at baseline were not significantly different between the two groups.

Three months after the implantation, two-dimensional echocardiography showed significant improvement of the

Copyright © Lippincott Williams & Wilkins. Unauthorized reproduction of this article is prohibited.

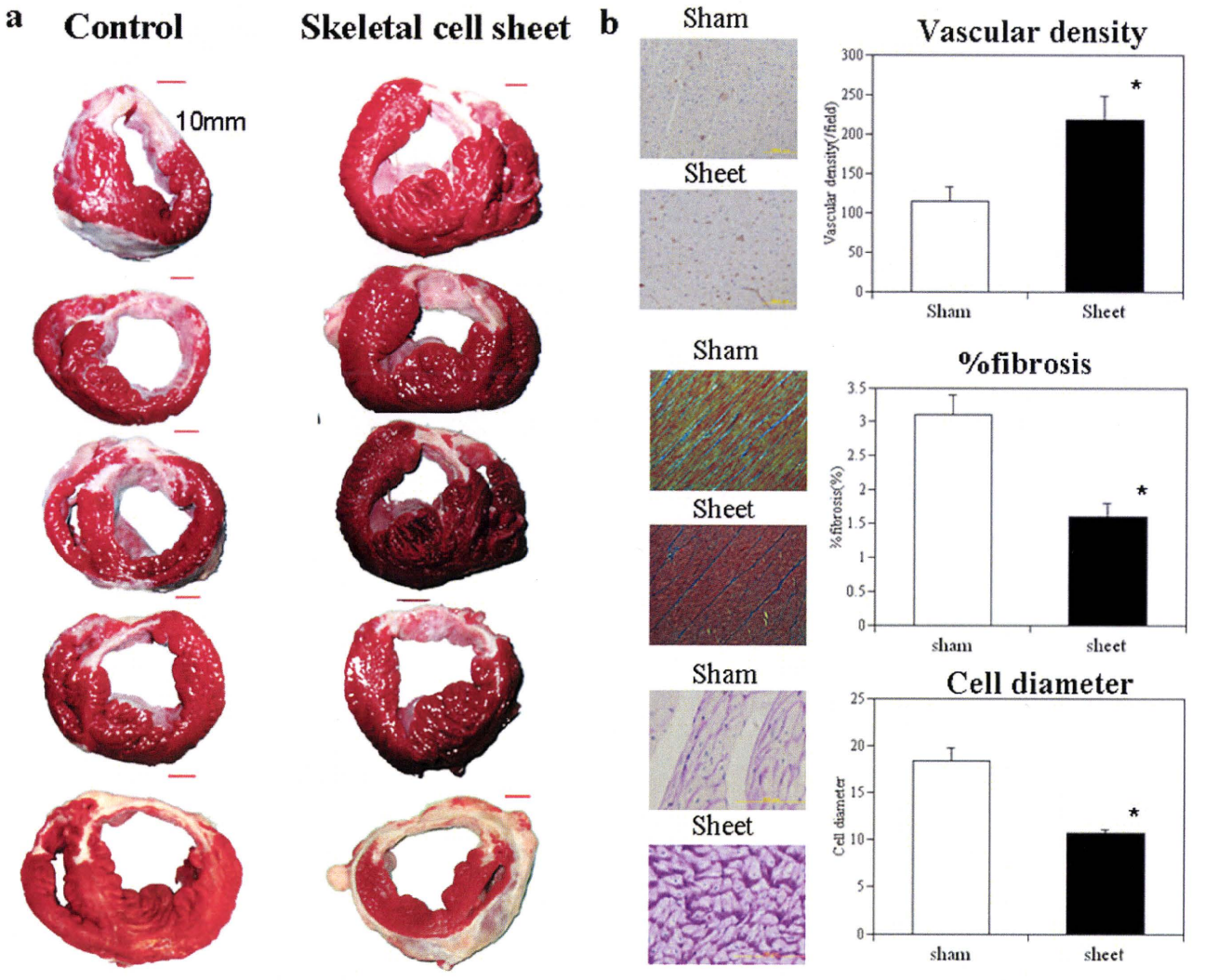

FIGURE 3. Macroscopic images of impaired myocardium receiving skeletal cell (SC) sheets and histological evaluation. (a) In the SC group, the anterior wall has recovered compared with the C group. In the SC group, the short axis area of the left ventricle (LV) is small compared with the C groups. In contrast, the C group shows a dilated LV and the anterior wall is thinner than in the SC groups. (b) Histological evaluation. Vascular density: the SC group showed a significant improvement in vascular density as assessed by immunostaining for the factor VIII-related antigen. *P less than 0.05 vs. C. The ratio of fibrosis-occupied area (% fibrosis) at a site remote from the infarcted heart region: picro-sirius red staining demonstrated that % fibrosis at a site remote from the infarcted heart region was significantly reduced in the SC group compared with the C group. *P less than 0.05 vs. C. The diameter of cardiomyocyte: the diameter of cardiomyocyte is significantly shorter in the SC group than the C group. *P less than 0.05 vs. C.

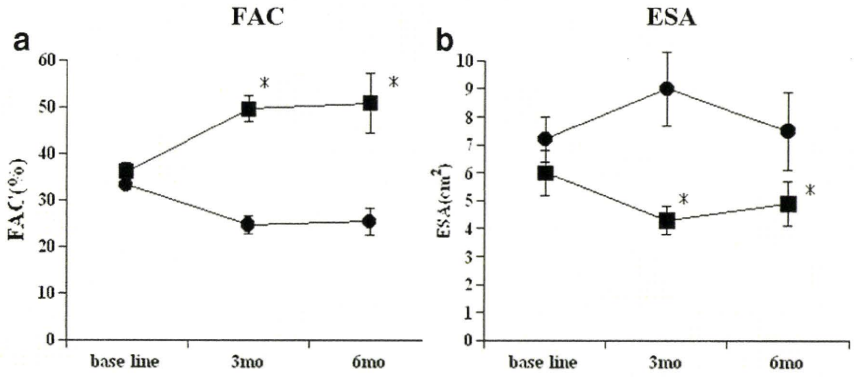

FIGURE 4. Global functional effects of infarcted myocardium receiving the implant. Global systolic function assessed by the fractional area shortening (FAS) (a) was significantly improved in the skeletal cell (SC) group 3 months after transplantation, and these functional improvements were preserved 6 months after SC sheet implantation. (b) The end-systolic area (ESA) was significantly smaller in the SC group than in the C groups 3 and 6 months after implantation. *P less than 0.05 vs. C, ■: SC sheet, ●: control.

Copyright © Lippincott Williams & Wilkins. Unauthorized reproduction of this article is prohibited.

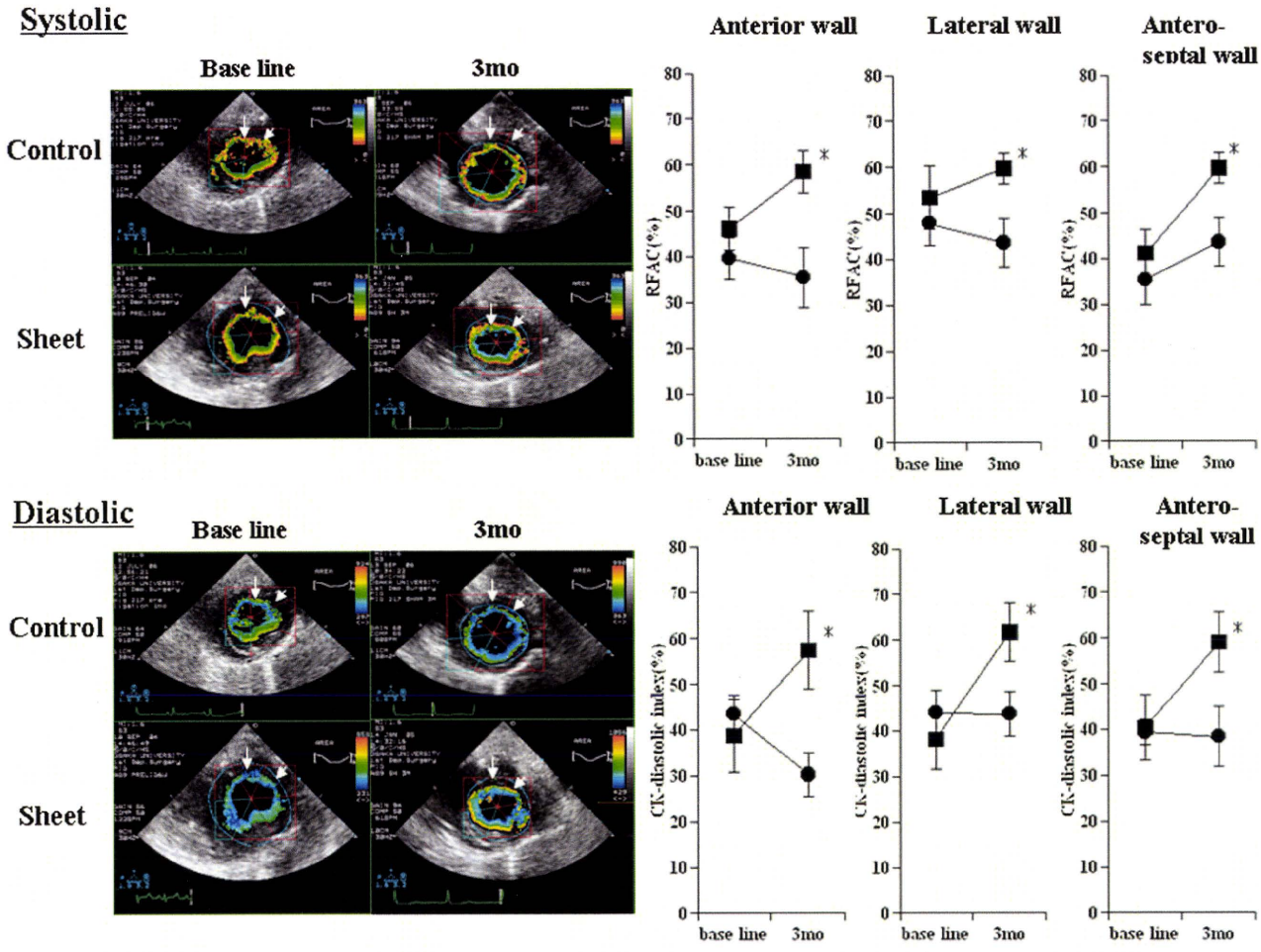

FIGURE 5. Systolic function: regional systolic function was significantly recovered in the skeletal cell (SC) group 3 months after implantation compared with the C group in the anterior, lateral, and anteroseptal wall. *P less than 0.05. Diastolic function: regional dysfunction was significantly recovered in the SC group 3 months after implantation compared with the C group in the anterior, lateral, and anteroseptal wall. Before treatment, diastolic dysfunction was observed in the infarction area of myocardium and the regional delayed relaxation was detected in the remote site of infarction by color kinesis. But this phenomenon was disappeared after SC sheet implantation. *P less than 0.05, ■: SC sheet, ●: control.

FAS (Fig. 4a) in the SC group compared with the C group (SC vs. C=49.5±2.8 vs. 24.6±2.0%, $P<0.05$). These functional improvements were preserved 6 months after implantation (SC vs. C=50.8±6.4 vs. 25.3±2.8%, $P<0.05$). The ESA was significantly smaller in the SC group than in the C group 3 months after the implantation (SC vs. C=4.3±0.5 vs. 9±1.3 cm^2, $P<0.05$) (Fig. 4b). These attenuation of LV dilatation were preserved 6 months after implantation (SC vs. C=4.9±0.8 vs. 7.5±1.4 cm^2, $P<0.05$). During this long-term observation, all SC sheet-treated animals were alive and exhibited no malignant arrhythmia assessed by 24-hour Holter ECG once a week (data not shown).

Before treatment, diastolic dysfunction was observed in the infarction area of myocardium and the regional delayed relaxation was detected in the remote site of infarction by color kinesis. After 3 months after implantation, CK-diastolic index in the lateral (SC vs. C=61.7±6.4 vs. 43.7±4.8%, $P<0.05$), anterior (SC vs. C=57.4±8.6 vs. 30.2±4.7%, $P<0.05$), and anteroseptal (SC vs. C=59±6.6 vs. 38.4±6.6%, $P<0.05$) segment were significantly ameliorated in the SC group compared with the C group, and regional systolic function in transplanted site was significantly improved in the SC group while not in the C groups (SC vs. C: lateral, 59.8±3.3 vs. 43.6±5.4%, $P<0.05$; anterior, 58.5±4.5 vs. 35.4±6.6%, $P<0.05$; anteroseptal, 59.8±3.3 vs. 43.6±5.4%, $P<0.05$), respectively (Fig. 5).

We could detect no ventricular premature beat for 24 hr by the Holter ECG in three myocardial infarction porcine received SC sheets.

Regional Myocardial Blood Flow and Residual Myocardial Tissue

PET study by using ^{15}0-water showed that the myocardial water-perfusable tissue fraction and myocardial blood flow were higher in the anterior wall where SC sheets were implanted compared with the myocardium receiving no sheets. These data depict that myocardial blood flow was better and microcirculation in the infarcted myocardium was preserved in the SC sheets implanted myocardium. PET study by using ^{18}F-FDG revealed that more viable myocardial tis-

Copyright © Lippincott Williams & Wilkins. Unauthorized reproduction of this article is prohibited.

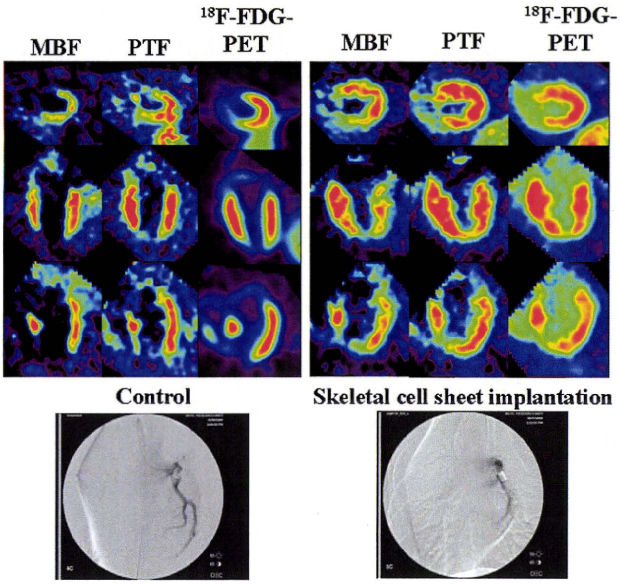

FIGURE 6. Positron emission tomography (PET) study revealed that perfusable tissue fraction (PTF) and myocardial blood flow (MBF) were higher and more viable myocardial tissues were preserved in the skeletal cell sheets implanted site compared with the myocardium receiving no sheets.

sues were preserved in the skeletal sheet implanted myocardium compared with the myocardium receiving no sheets. Coronary angiography revealed that LAD was occluded by the ameroid constrictor in both cases (Fig. 6).

DISCUSSION

Over the past several years, increasing awareness of the shortcomings of heart transplantation and left ventricular assist system implantation has led cardiovascular surgeons to consider alternative means of treating end-stage heart failure. In clinical setting, cellular cardiomyoplasty has been reported to have the potential of fundamental regenerative capability and has already been introduced in clinical trials with skeletal myoblast (*11*) or bone marrow mononuclear cells (*12*), and results suggest that it is a relatively feasible and safety therapy as a therapeutic angiogenesis. In this setting, cardiac tissue implantation was proposed to the treatment of end-staged heart failure as a new concept of regenerative therapy and experimentally some groups depicted it's effectiveness in the damaged myocardium (*13*, *14*). We also reported that cell sheets have great impacts on restoration of damaged myocardium in the rat infarction model (*3*, *4*) and dilated cardiomyopathy hamster (*5*). To convince the effectiveness of cell sheets in preclinical trial, we examined whether autologous SC sheets implantation might become one of the armamentarium of regenerative therapy for chronic heart failure caused by myocardial infarction in the porcine model.

The potential added advantages of the cell sheet implantation method include the implantation of a high number of cells with minimum cell loss. In contrast, the injection method is associated with a high loss of cells or surface proteins due to the trypsin treatment. Despite a high number of cell loss in needle injection, the cell sheet implantation method might provide the advantages of a higher number of cell implantation without cellular community destruction, leading the more improvement of cardiac performance rather than cell injection method (*4*). In case of needle injection, inflammation accompanied with destruction of myocardium induced by needle injection promotes graft death after cell transplantation (*15*).

To examine the effects of the SC sheet implantation therapy, we analyzed cardiac function and performed a histological assessment of the infarcted heart after SC sheet transplantation in a swine infarction model. SC sheet implantation therapy significantly induced angiogenesis, reduction of fibrosis histologically. And cell diameter of host myocyte was significantly attenuated its hypertrophy compared with the no treatment group. PET study revealed the better regional blood perfusion and better regional myocardial viability in the myocardium receiving cell sheets compared with the myocardium receiving no sheets.

Moreover, SC sheet implantation induced functional recovery of damaged myocardium. Especially, we demonstrated that the regional diastolic and systolic dysfunction was well recovered in the sheet implanted group. Before treatment, diastolic dysfunction of infarcted area and regional delayed relaxation of noninfarcted site were detected by color kinesis in the porcine infracted myocardium. After treatment, diastolic dysfunction of infarcted site was significantly recovered and the phenomenon of regional delayed relaxation in noninfarcted site was not seen. Presumably, implanted elastic myoblast sheets and a large quantity of well-developed smooth muscle cells, which are detected in the center of the scar, improved the regional diastolic dysfunction of implanted site. Although SC sheet can not contract in vivo after implantation, this recovery of diastolic disassociation of LV might result in the recovery of systolic dysfunction.

To the best of our knowledge, this is the first report in which tissue-engineered SC sheets implantation was successfully used to improve cardiac performance in a large animal model of ischemic myocardium according to the Laplace's theory.

The mechanisms of the restoration of damaged myocardium by SC sheet implantation might be complicated and many pathways might affect the recovery of ischemic myocardium. Recent reports depict that cell sheets enhance the recruitment of hematopoietic stem cells through the release of stromal-derived factor 1 (*4*). The fact of thicker anterior wall and the improvement of regional function might depend on both the recruitment of cytokine releasing stem cells, survival of grafted cells, and well-developed smooth muscle cells. And these cells might have good elasticity and these elastic cells and tissues softened the stiffness of anterior wall in association with the attenuating fibrosis even in the infarct area. This reduced stiffness of anterior wall might lead to the improvement of the diastolic dysfunction. Transplanted SCs cannot differentiate into cardiomyocyte anymore, but regional systolic function improved in the transplanted site. Probably, the improvement of regional diastolic function due to elastic cells might be responsible for the restoration of regional systolic dysfunction. Recent reports demonstrated that regional left ventricular myocardial relaxation was closely related to regional myocardial contraction (*16*) and the improvement of regional myocardial relaxation leads to the

Copyright © Lippincott Williams & Wilkins. Unauthorized reproduction of this article is prohibited.

recovery of global diastolic function (*17*). Moreover, the improvement of regional systolic function is closely related to global systolic function (*18*). We assume that this theory about the relationship between diastolic and systolic function is one of the mechanisms about the improvement of diastolic and systolic function in the cell sheet transplanted myocardium.

Question is why the well-developed smooth muscle cells exist in the center of the scar in the SC sheet group after transplantation despite a small quantity of smooth muscle cells in the SC sheet? Does a small quantity of smooth muscle cells in the SC sheet proliferate after transplantation? Do progenitor cells in the SC sheet differentiate to smooth muscle cells? Do progenitor cells or smooth muscle cells in the host myocardium migrate to the implanted site and proliferate? To the regret, there is no data to answer these questions exactly in this article and more detailed studies are needed to elucidate this important question.

Some reports depicted that the expression of hepatocyte growth factor (HGF) in the myoblast sheet transplanted ischemic myocardium is higher compared with the nontransplanted ischemic myocardium (*4*). HGF has an antifibrotic activity both through the activation of a matrix degradation pathway (*19*), restoration of cytoskeletal proteins on cardiomyocyte (*20*), and induce angiogenesis in the ischemic myocardium (*21*). Our study demonstrated that % fibrosis was significantly reduced in the SC sheet transplanted group. This paracrine secretion of HGF from SC sheets might attribute the reduction of % fibrosis. In our study, much more factor VIII-positive cells are detected in the SC sheet transplanted myocardium. This might be induced by paracrine secretion of HGF and angiogenesis might rescue the ischemic host cardiomyocyte and bring about the improvement of the distressed function of host cardiomyocyte. The distressed cytoskeletal proteins on the cardiomyocyte in the ischemic myocardium might be reorganized by the HGF secreted from skeletal sheet and the restoration of cytoskeletal proteins might lead to the improvement of cardiac function. And some reports demonstrated that myoblast sheets maintain the distressed cytoskeletal proteins on the host cardiomyocyte in the dilated cardiomyopathy hamster model (*5*). Consequently, cell sheet treatment is appropriate for recovery of ischemic cardiomyopathy. Recent research works demonstrated that several regenerative factors such as insulin-like growth factor-1 (*22*) and Thymosin b4 (*23*) were expressed in the rat ischemic myocardium model after myoblast sheet implantation by reverse-transcriptase polymerase chain reaction analysis (data not shown). After myoblast sheet transplantation to ischemic myocardium, several regenerative factors are expressed in the transplanted site, and these long-term and low-dosed expressed regenerative factors might cooperatively restore the damaged myocardium.

We could find no ventricular premature beat analyzed by Holter ECG after SC sheet implantation. We have already proved that in the rat infarction model, arrhythmia is less in the SC sheet implantation group compared with the needle injection group and this work represented that more monocyte chemotactic protein-1-positive cells and CD11b (macrophage marker)-positive cells were detected in the needle injection group compared with SC sheet implantation (data not shown). We speculate that needles destroy the myocardium and this destroyed myocardium may induce the inflammation and this inflammation may induce the arrhythmia. Conversely, SC sheet implantation technique normally doses not destroy the myocardium when they are implanted to recipient heart. Moreover, SC sheet will survive on the epicardium and electrical wave originated from implanted myoblasts may not deliver to the recipient myocardium directly. But when we implant myoblasts by needle injection, implanted myoblasts survive in the center of the myocardium and electrical wave will deliver to the myocardium directly, leading to the arrhythmia.

In conclusion, we have preclinically demonstrated SC sheets produced histologically and functionally apparent prevented the deterioration of the impaired myocardium in the swine model. These data provide a basis for attempting clinical cell sheet implantation in ischemic disease as the armamentarium to promote the regeneration of chronic heart failure caused by myocardial infarction.

ACKNOWLEDGMENTS

The authors thank Shigeru Matsumi and Masako Yokoyama for their excellent technical assistance.

REFERENCES

1. Shimizu T, Yamato M, Akutsu T, et al. Fabrication of pulsatile cardiac tissue grafts using a novel 3-dimensional cell sheet manipulation technique and temperature-responsive cell culture surfaces. *Circ Res* 2002; 90: e40.
2. Shimizu T, Sekine H, Isoi Y, et al. Long-term survival and growth of pulsatile myocardial tissue grafts engineered by the layering of cardiomyocyte sheets. *Tissue Eng* 2006; 12: 499.
3. Miyagawa S, Sawa Y, Sakakida S, et al. Tissue cardiomyoplasty using bioengineered contractile cardiomyocyte sheets to repair damaged myocardium: Their integration with recipient myocardium. *Transplantation* 2005; 80: 1586.
4. Memon IA, Sawa Y, Fukushima N, et al. Repair of impaired myocardium by means of implantation of engineered autologous myoblast sheets. *J Thorac Cardiovasc Surg* 2005; 130: 1333.
5. Kondoh H, Sawa Y, Miyagawa S, et al. Longer preservation of cardiac performance by sheet-shaped myoblast implantation in dilated cardiomyopathic hamsters. *Cardiovasc Res* 2006; 69: 466.
6. Hata H, Matsumiya G, Miyagawa S, et al. Grafted skeletal myoblast sheets attenuate myocardial remodeling in pacing-induced canine heart failure model. *J Thorac Cardiovasc Surg* 2006; 132: 918.
7. Mor-Avi V, Vignon P, Bales AC, et al. Acoustic quantification indexes of left ventricular size and function: Effects of signal averaging. *J Am Soc Echocardiogr* 1998; 11: 792.
8. Ishii K, Miwa K, Makita T, et al. Prolonged postischemic regional left ventricular delayed relaxation or diastolic asynchrony detected by color kinesis following coronary vasospasm. *Am J Cardiol* 2003; 91: 1366.
9. Fukui S, Kitagawa-Sakakida S, Kawamata S, et al. Therapeutic effect of midkine on cardiac remodeling in infarcted rat hearts. *Ann Thorac Surg* 2008; 85: 562.
10. Iida H, Yokoyama I, Agostini D, et al. Quantitative assessment of regional myocardial blood flow using oxygen-15-labelled water and positron emission tomography: A multicentre evaluation in Japan. *Eur J Nucl Med* 2000; 27: 192.
11. Dib N, Michler RE, Pagani FD, et al. Safety and feasibility of autologous myoblast transplantation in patients with ischemic cardiomyopathy: Four-year follow-up. *Circulation* 2005; 112: 1748.
12. Perin EC, Dohmann HF, Borojevic R, et al. Transendocardial, autologous bone marrow cell transplantation for severe, chronic ischemic heart failure. *Circulation* 2003; 107: 2294.
13. Leor J, Aboulafia-Etzion S, Dar A, et al. Bioengineered cardiac grafts. A new approach to repair the infarcted myocardium? *Circulation* 2000; 102(suppl III): III-56.

Copyright © Lippincott Williams & Wilkins. Unauthorized reproduction of this article is prohibited.

14. Li RK, Jia ZQ, Weisel RD, et al. Survival and function of bioengineered cardiac grafts. *Circulation* 1999; 100(suppl II): II-63.
15. Suzuki K, Murtuza B, Beauchamp JR, et al. Role of interleukin-1beta in acute inflammation and graft death after cell transplantation to the heart. *Circulation* 2004; 110(11 suppl 1): II-219.
16. Tanaka H, Kawai H, Tatsumi K, et al. Relationship between regional and global left ventricular systolic and diastolic function in patients with coronary artery disease assessed by strain rate imaging. *Circ J* 2007; 71: 517.
17. Tanaka H, Kawai H, Tatsumi K, et al. Improved regional myocardial diastolic function assessed by strain rate imaging in patients with coronary artery disease undergoing percutaneous coronary intervention. *J Am Soc Echocardiogr* 2006; 19: 756.
18. Moller JE, Hillis GS, Oh JK, et al. Wall motion score index and ejection fraction for risk stratification after acute myocardial infarction. *Am Heart J* 2006; 151: 419.
19. Liu Y, Rajur K, Tolbert E, et al. Endogenous hepatocyte growth factor ameliorates chronic renal injury by activating matrix degradation pathways. *Kidney Int* 2000; 58: 2028.
20. Miyagawa S, Sawa Y, Taketani S, et al. Myocardial regeneration therapy for heart failure: Hepatocyte growth factor enhances the effect of cellular cardiomyoplasty. *Circulation* 2002; 105: 2556.
21. Taniyama Y, Morishita R, Aoki M, et al. Therapeutic angiogenesis induced by human hepatocyte growth factor gene in rat and rabbit hindlimb ischemia models: Preclinical study for treatment of peripheral arterial disease. *Gene Ther* 2001; 8: 181.
22. Li Q, Li B, Wang X, et al. Overexpression of insulin-like growth factor-1 in mice protects from myocyte death after infarction, attenuating ventricular dilation, wall stress, and cardiac hypertrophy. *J Clin Invest* 1997; 100: 1991.
23. Bock-Marquette I, Saxena A, White MD, et al. Thymosin beta4 activates integrin-linked kinase and promotes cardiac cell migration, survival and cardiac repair. *Nature* 2004; 432: 466.

e-TOCs and e-Alerts

Receive the latest developments in transplantation as soon as they're available.

Request the delivery of *Transplantation's* e-Alerts directly to your email address. This is a fast, easy, and free service to all subscribers. You will receive:

- Notice of all new issues of *Transplantation,* including the posting of new issues at the *Transplantation* website
- Complete Table of Contents for all new issues

Visit www.transplantjournal.com and click on e-Alerts.

Copyright © Lippincott Williams & Wilkins. Unauthorized reproduction of this article is prohibited.

再生医療・細胞治療の規制に関する国際動向

Regulation of Cell Therapy Products and Tissue Engineered Products in EU and USA

佐藤 陽治　国立医薬品食品衛生研究所・遺伝子細胞医薬部・第2室　室長

〒158-8501 東京都世田谷区上用賀1-18-1　Tel：03-3700-1141（代）　Fax：03-3707-6950
E-mail：yoji@nihs.go.jp

1　細胞・組織加工製品

治療法に乏しく，重篤・致死的ないしQOLを著しく損なう疾病・損傷に対する活路として，再生医療や細胞治療には非常に大きな期待が集まっている。これらの先進的な医療に用いることを目的として加工（培養・活性化・足場との複合化等）を施された細胞や組織，あるいは加工された細胞・組織を含む製品は「細胞・組織加工製品」（細胞・組織加工医薬品ないし細胞・組織加工医療機器）と呼ばれ，その開発は世界的にも熾烈な競争が展開している。ただし細胞・組織加工製品は，細胞という動的で複雑な成分を含むと同時に，その臨床応用に関して限られた経験と知識しか存在しないため，明確な科学的根拠に基づいた品質や安全性等の確保が課題となっており，比較的進んでいると言われる欧米においても，当局は実用化を促進するための試行を繰り返しながら規制の枠組みの整備を進めている。

2　規制の原則

欧米における細胞・組織加工製品の規制の原則は「リスクベースアプローチ」と呼ばれ，目的とする製品の性質に固有，かつその品質・安全性・有効性に関連するリスクの分析をベースにし，その影響の度合いを科学的に評価することにより規制や開発の方針・内容を定めるアプローチ方法が採られている。日本では，細胞・組織加工製品を医薬品・医療機器として開発するために薬事法に則って実施される「治験」と，細胞・組織加工製品を用いた治療法の開発を目的として医療法・医師法のもとで行われる「臨床研究」という異なる規制の枠組みが存在するが，欧米ではリスクベースアプローチの原則に基づき，商業目的か非商業目的かに拘わらず，原則的には同一の規制がかかる。即ち，大学病院等による非商業目的の「臨床研究」においても国への臨床試験申請並びにICH-GCP準拠が要求される点で日本よりも厳しい制度となっている。それでも開発が進む理由としては，研究資金・臨床試験支援体制などが充実している他，規制当局等の専門家が開発早期から開発者と情報を共有し，製品の目的に沿った柔軟な対応が可能となっていることなどが挙げられる。

3　EUの規制

欧州連合（EU）では細胞・組織加工製品は，製品中に含まれる細胞の作用様式に基づき体細胞治療薬（薬理学的・免疫学的又は代謝的機能）または組織工学製品（ヒト組織の再生・修復又は置換）に分類される。従来，体細胞治療薬は遺伝子治療薬とともにATMP（advanced therapy medicinal product）という医薬品の一類型に分類されていたが，2008年12月の制度改正により組織工学製品もATMPとして医薬品の規制を受けることになった。これと同時に，ATMPの販売承認については加盟国における審査を経ずに欧州医薬品庁（EMA）による中央審査によって行われるようになっており，制度改正からこれまでに培養軟骨製品1品目がATMPとして販売承認を受けている。なお制度改正以前に販売承認を